

Toward a multi-scale model of antigen presentation in immunity

Denise E. Kirschner^{1,2}, Stewart T. Chang¹, Thomas W. Riggs¹, Nicolas Perry¹, Jennifer J. Linderman^{2,3}

¹Department of Microbiology and Immunology, University of Michigan Medical School, Ann Arbor, MI, USA

²Department of Biomedical Engineering, University of Michigan, Ann Arbor, MI, USA

³Department of Chemical Engineering, University of Michigan, Ann Arbor, MI, USA

Correspondence to:

Denise E. Kirschner

Department of Microbiology and Immunology

University of Michigan Medical School

6730 Medical Science Building II

Ann Arbor, MI 48109, USA

Tel: +1 734 647 7722

Fax: +1 734 647 7723

E-mail: kirschne@umich.edu

Computer system: Windows

Word processor: Microsoft Word

Summary

The immune system and the process of antigen presentation in particular encompass events that occur at multiple length and time scales. Despite a wealth of information in the biological literature regarding each of these scales, no single representation synthesizing this information into a model of the overall immune response as it depends on antigen presentation is available. In this paper we outline an approach for integrating information over relevant biological and temporal scales to generate such a representation for MHC class II-mediated antigen presentation. In addition, we begin to address how such models can be used to answer questions about mechanisms of infection and new strategies for treatment and vaccines.

Introduction

Biological systems are often explored in the laboratory at a reductionist scale. The idea is that if we understand everything at particular scales (most recently focused at the molecular scale), we will then understand the system as a whole; immunology is no exception. Of concern, however, is that the immune system spans multiple length (gene through body) and time (sub-second through lifetime) scales and that the immune response will likely only be completely understood through knowledge of how processes at these different scales work together. Such an integrative picture of a system is the desired outcome of multi-scale modeling. In total, approaches that capture multi-scale or system-wide features fall under the umbrella of systems biology.

Systems biology encourages a non-reductionist approach to model development, beginning with the simplest possible model. Coined ‘reconstructionism’ by M. Savageau (1), the idea is that biological systems are more than the sum of their parts and that integrative behavior occurs in a non-predictable fashion. The modeling process itself brings about an understanding of the underlying system, as components are captured with mathematics and/or statistics. A minimal model is constructed and then grows in complexity, driven by new hypotheses that may not have been apparent from the phenomenological descriptions. With recent advances in information technology—fast and inexpensive computing power, global networking infrastructure, and comprehensive databases—modeling and simulation are becoming increasingly important biological tools. For the most part these efforts have focused at a single scale, e.g. genomic/proteomic, cellular, tissue, organ, organ system and whole body. Only now is there an emphasis to develop tools, techniques, algorithms, and mathematical theory to integrate seamlessly the continuum from the micro- to the macro-scale. Multi-scale modeling deals with spanning scales as diverse as from molecular to population. It can impact our understanding of biological processes and also further our predictive capabilities in biology. Multi-scale algorithms are built and validated against experimentally derived data and observations.

The need for multi-scale approaches in biology is recognized in the cardiovascular field, where a number of groups are developing methods to integrate molecular and cellular events with organ function (e.g. 2, 3). In addition, multi-scale approaches are now being considered for neural systems (4, 5, 6), tumor growth (7), the vasculature (8), and developmental biology (9). Multi-scale approaches are also being applied in various engineering problems, for example in polymer science (10) and tissue engineering (11). We argue that immunology is also ripe for such a multi-scale approach.

We focus in this chapter on antigen presentation via the major histocompatibility complex class II (MHC II) pathway and its role in the immune response. We first review the relevant biological events and discuss the multi-scale aspects of the process. We then present models that have been developed to address biological events occurring at various scales and give examples of applications to the study of disease dynamics. Finally we discuss ways to begin to integrate models across scales.

The biology of antigen presentation

Antigen presentation is the process by which peptide fragments from the proteins of pathogens or the host are partially degraded and then displayed (or “presented”) on the surfaces of cells in complex with MHC molecules. Once bound to MHC, antigens can be recognized by cognate T cells which then respond by either killing the original antigen-presenting cell or else activating it along with other cells. While antigen presentation may appear to occur only at molecular and cellular scales, events at other scales also affect the outcome. For instance, antigen presentation to naïve T cells occurs within the larger context of the lymph node (LN), and other chemical signals (e.g. cytokines produced by other cells) within the LN or the topology of the LN itself may affect whether APCs are able to contact and activate T cells. Similarly, the ability of effector T cells to traffic out of the LN and throughout the body will affect the time course of an infection. The success of antigen presentation therefore depends on events occurring at multiple biological scales (*Fig. 1*).

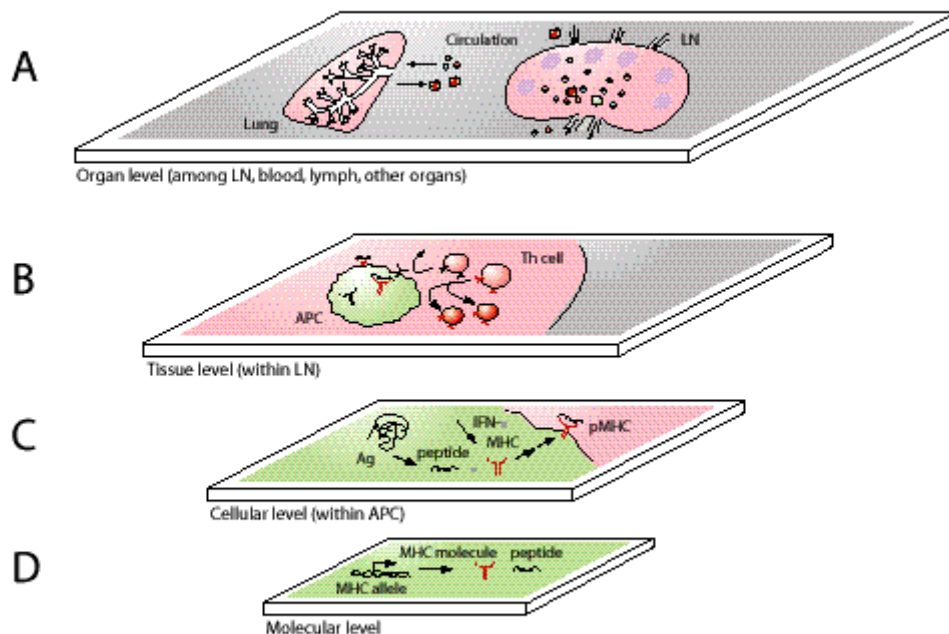


Figure 1

Peptide-MHC binding

A key event in antigen presentation is the binding of peptide to one of two classes of MHC molecule. All nucleated human cells perform antigen presentation to some extent by expressing MHC class I (MHC I) molecules which sample peptides from the

cytoplasm. However, some cells are also capable of presenting peptides derived from exogenous antigens using MHC class II molecules; these specialized cells are known as professional antigen-presenting cells (APC). In this review we focus macrophages and dendritic cells, although B cells can also serve as APCs. (A recently discovered pathway for presenting lipid antigens, the CD1 pathway, will not be considered here. See (12) for a review of this topic.)

For the most part the two classes of MHC molecule sample different sources of antigen and take divergent pathways through the cell. Proteins found in the cytoplasm, including those produced by viruses, are degraded (or “processed”) into shorter peptides by the main protein turnover machinery of the cell, the proteasome. A subset of these peptides is transported into the endoplasmic reticulum (ER) by the transporter associated with antigen processing (TAP). Binding between peptides of a particular length (8-10 amino acids) and MHC class I molecules then occurs within the ER, and the resulting complexes are trafficked to the cell surface. In contrast antigens from pathogens that do not reside in the cytoplasm, including bacteria and parasites, are generally first taken up by the cell and then processed in the endosomal pathway. Cathepsin proteases located within the endosomal pathway become activated by the increasingly acidified environment and cleave the protein antigens into peptides of shorter lengths. Binding between extracellular-derived peptides of varying lengths (often greater than 9 amino acids) and MHC class II molecules then occurs later in this pathway or in a specialized vacuole that branches off known as the MHC class II binding compartment (MIIC). Peptide-MHC II complexes are then trafficked to the cell surface as in the case of the class I pathway. In both cases the final stage is recognition of the complexes by cognate T cell receptors (TCR), either on the surface of CD8⁺ cytotoxic T cells (in the case of MHC class I) or on the surface of CD4⁺ helper T cells (in the case of MHC class II).

One theme that arises from this cursory overview of both antigen presentation pathways is the importance of high-affinity binding. Peptides that bind a particular MHC molecule weakly—or alternatively MHC variants that bind a particular peptide weakly—are expected to lead to relatively few peptide-MHC complexes on the APC surface. Binding affinities of peptide-MHC complexes can be measured *in vitro* using a number of different techniques. In the most common assay, a competitive binding assay, various concentrations of the peptide of interest are used to displace the binding of a labeled reporter peptide. The concentration at which 50% of the reporter peptide is displaced provides the IC_{50} which approximates the equilibrium dissociation constant of a peptide-MHC complex, K_D . More precisely IC_{50} is related to K_D according to

$$K_D = IC_{50} (1 + L_r/K_r)^{-1}$$

where L_r and K_r represent the concentration of the reporter peptide and the equilibrium dissociation constant of the reporter peptide-MHC complex, respectively (13). These parameters frequently vary by protocol, L_r explicitly so and K_r by virtue of being specific to each combination of peptide and MHC (14, 15, 16). Alternatively K_D values and even association and dissociation rate constants can be determined by other techniques including radiolabeling and fluorescence polarization methods (17). Several online

databases including MHCPEP (18), MHCBN (19), and AntiJen (20) now store peptide-MHC binding affinities. These databases currently contain measurements on approximately 13000, 14000, and 24000 peptides, respectively. In the former two databases IC_{50} values are not available directly but can be inferred from the four-tiered classification used by both databases: high affinity indicates IC_{50} of <1 nM; moderate, IC_{50} of 1 nM-100 nM; low, IC_{50} of 100 nM-10 μ M; no binding, IC_{50} of >10 μ M. An IC_{50} of 500 nM is also commonly used as a threshold to differentiate binding from non-binding (21). In AntiJen IC_{50} is reported directly whenever possible.

The greater significance of binding affinity to antigen presentation can also be discerned from the epidemiological literature. Various MHC alleles have been correlated with increased susceptibility to diseases, particularly chronic diseases of an autoimmune or infectious nature (22). Examples of diseases associated with particular MHC alleles include type I diabetes, rheumatoid arthritis, malaria, and tuberculosis. Because most polymorphisms in MHC molecules occur within the peptide-binding region, it is reasonable to assume that binding to either peptide or TCR is affected. The detailed mechanisms behind these associations have not yet been elucidated, although several hypotheses exist (22, 23, 24). Furthermore a correlation between peptide-MHC affinity and magnitude of the immune response at the cellular level has been demonstrated (25, 26). We provide a full treatment of this topic elsewhere (Chang *et al.*, in preparation).

Cellular processes controlling display of peptide-MHC complexes

Peptide-MHC binding is by no means the only step that is regulated in the antigen presentation pathway. Other steps are controlled dynamically—by cell-to-cell contact or the constantly changing cytokine environment surrounding the APC, for instance—and allow antigen presentation to be fine-tuned. We describe these steps and others relevant to the MHC II-mediated pathway in more detail below (*Fig. 2*) but refer the reader to a recent review for a full treatment (27).

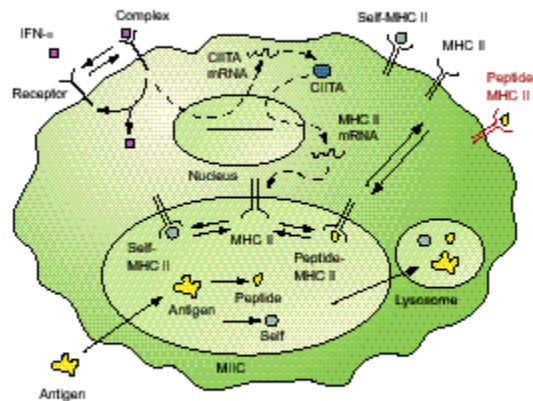


Figure 2

Antigens for the MHC II-mediated pathway are generally internalized by one of three routes before converging on the endosomal pathway: phagocytosis, fluid-phase pinocytosis, and receptor-mediated endocytosis. Internalized antigens then progress through increasingly acidified endosomes and are exposed to low pH-activated cathepsins that degrade the antigens into smaller peptides (28). These peptides then either bind MHC II molecules or are directed to lysosomes for degradation.

MHC II expression normally occurs at low levels in resident APCs but can be up- or down-regulated by the cytokine environment. Interferon- γ (IFN- γ) is one cytokine that affects MHC class II expression. After IFN- γ binds to its receptor on the APC surface, a signal is propagated through the JAK-STAT pathway that increases the level of class II transactivator (CIITA) in the cell. CIITA acts as the master regulator of MHC II transcription, and increased levels of CIITA lead to parallel increases in MHC II expression several hours after exposure to IFN- γ . Nascent MHC II molecules enter the ER and are coupled to another protein, invariant chain (Ii). The luminal domain of Ii binds the peptide-binding groove of MHC II, protecting it from proteases, while the cytoplasmic domain of Ii directs the two molecules to the endosomal pathway. After reaching the endosomal pathway MHC II molecules retain a remnant of Ii, the class II invariant peptides (or CLIP), until released by the enzyme H2-/HLA-DM (29). Here antigenic peptides compete for binding to MHC II with self peptides that are present at high levels and may bind greater than 80% of the available MHC II in the absence of exogenous peptides (30, 31). In complex with either self or exogenous peptides, MHC II molecules then traffic to the cell surface where they may remain stable for days until recognized by CD4⁺ T cells or internalized and degraded.

Macrophages and dendritic cells (DCs) express not only MHC II molecules but also co-stimulatory and adhesion molecules necessary to engage T cells. Both macrophages and DCs derive from a common precursor, the monocyte, which differentiates into one of the two cell types based on environmental cues (32, 33). (B cells, another APC type and not a focus of this review, are derived from hematopoietic cells in the bone marrow (27). Macrophages and DCs are found in overlapping distributions within the body in areas such as the LNs, and there is even evidence to suggest these cells can re-differentiate from one class to the other (34).

Differences between macrophages and DCs occur in the rates at which they perform processes related to antigen presentation. DCs express 10-100 times the number of MHC II molecules expressed by macrophages and also perform antigen uptake at generally increased rates (35, 36). Consistent with these findings, fewer DCs are required to activate T cells than macrophages (35). More importantly these cells play different roles in the overall development of the immune response. DCs take up antigen at the site of infection and migrate to LNs to present antigen, while macrophages primarily perform their function as APC at the infection site (37).

Cellular interactions in the context of the lymph node

Once on the surface of the APC, peptide-MHC II complexes (pMHC) can elicit partial or full activation of T cells depending at least in part on the number of peptides presented and the number of TCR engaged (i.e. bound to pMHC). Relatively few measurements of pMHC-TCR affinity have been made, although some are available in AntiJen (20). A single pMHC on the APC surface has been shown to be sufficient to elicit an intracellular release of calcium within the T cell, while full activation is generally acknowledged to require hundreds of complexes as gauged by the release of IL-2, a cytokine that initiates localized T cell division (also known as clonal expansion) (38, 39). In addition there is evidence that a quantitative relationship exists between surface pMHC levels and the magnitude of T cell response, assuming pMHC levels exceed a lower threshold (38, 40, 41, 42). The effects of antigen presentation may therefore be sensitive to variations in a number of contributing intracellular processes.

During the course of an infection antigen presentation occurs at two major sites. First, within the LN antigen presentation events that are responsible for initiating an adaptive immune response occur and are driven mainly by DCs. Secondly, at the site of infection macrophages participate in antigen presentation events that sustain immune responses. The tissue-level context strongly influences the dynamics of antigen presentation and recognition. For example, the LN environment restricts cytokines and chemokines to a microenvironment allowing efficient signaling to occur.

As the early events of immunity likely determine the success of the response, understanding events within the LN is a critical first step. There are approximately 700 LNs, each roughly 1-5 cm³ in size, distributed throughout the human body and those closest to a given site of infection will be engaged in infection dynamics. Some infections are systemic involving not a particular tissue site but instead the blood or multiple epithelial sites; in these cases many different LNs will be involved at some level.

LNs are connected through a series of lymphatics that serve as the highway between the LNs, entering into each LN through afferent lymph ducts and leaving through the medullary sinuses that flow into a single efferent lymph duct (*Fig. 3*). Blood vessels also feed into the lymphatic system, both directly into the LNs (at high endothelial venules: HEVs) and at junctures throughout. Lymphatics then return cells to blood via a common conduit: the thoracic duct (43). APCs circulate into LNs via the afferent lymphatics while T cells enter through the HEVs (44, 45). Once in the LN, CD4⁺ T cells sample the surface of APCs for pMHC complexes within the LN paracortex.

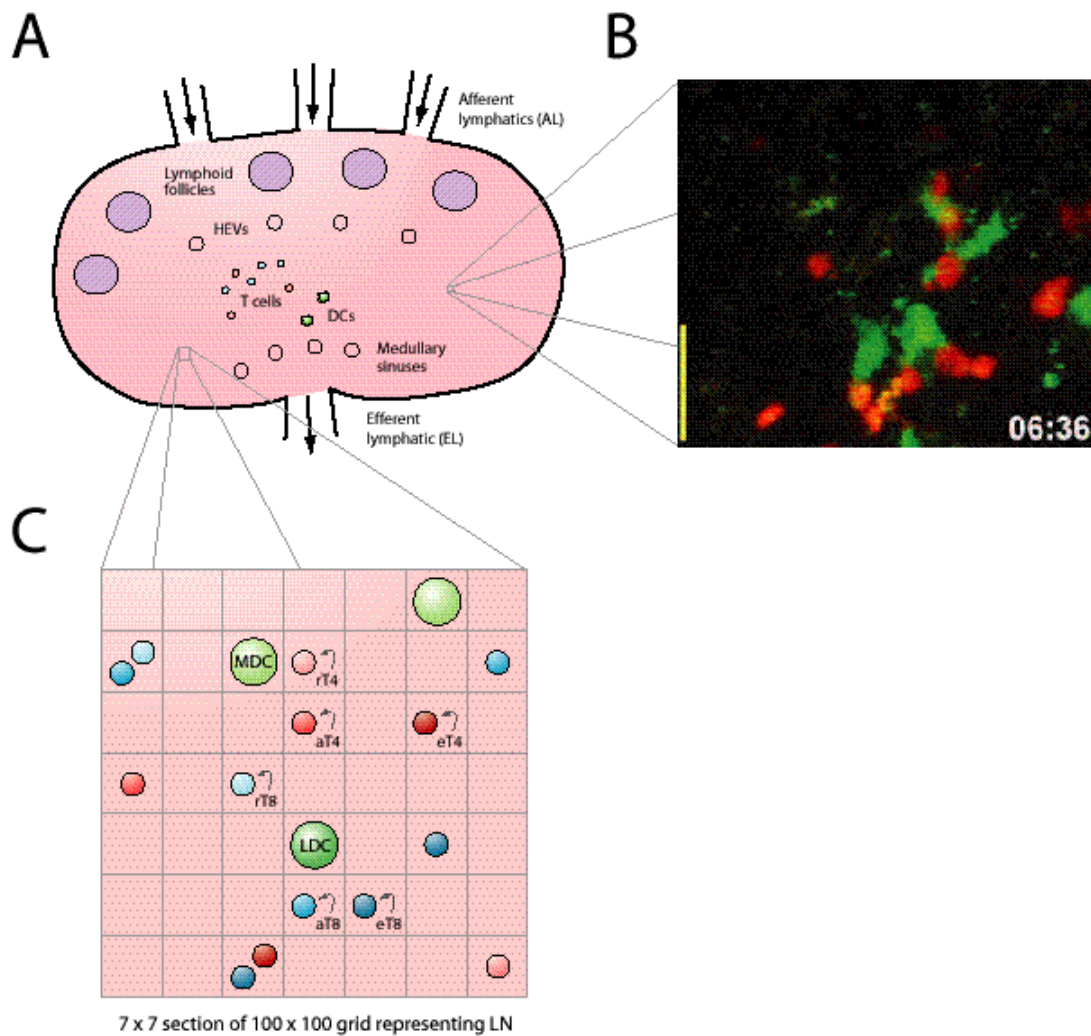


Figure 3

When a $CD4^+$ T cell encounters an APC and its TCR binds its cognate pMHC on the surface of the APC, a series of events follows leading to T cell activation. At the interface between APC and T cell, pMHC, TCR, and co-stimulatory and adhesion molecules aggregate into a structure known as the immunological synapse (IS) (46). Recently the IS has been the subject of intense investigation and several theories exist as to how this intricate structure forms and functions (e.g. 47). If recognition occurs, T cells become activated and begin secreting IL-2. These T cells differentiate and become fully activated in response to further environmental cues and additional cell-cell interactions with APCs (48, 49). Experimentally these changes can be tracked by measuring the amount of radioactively labeled nucleotide incorporated by T cells as they divide. The ability to quantify T cell activation in turn provides an assay for antigen presentation (50). In one commonly used *in vitro* assay, cultured APCs are pulsed with a particular model antigen (e.g. ovalbumin) and then exposed to T cell hybridoma cells specific for that antigen.

The composition of individual LNs can be determined by extracting the LNs from animals (pre- and post-infection) and analyzing them by flow cytometric methods (such as fluorescence-activated cell sorting, or FACS) (51, 52, 53, 54). From these studies it is clear that immune cell numbers increase dramatically during an immune response. However, what cannot be ascertained from these studies are the spatial dynamics that occur within a LN and are known to play a role in the success of antigen presentation events.

With the advent of two-photon intravital microscopy, a technique that allows visualization of cells within a tissue environment, it is becoming increasingly clear that T cell responses in LNs *in vivo* are much different than what has been observed *in vitro* due to environmental factors as well as the inherent structure of the LN (e.g. 55, 56; 57 and see *Fig. 3*). Using intravital techniques, one can observe T cells and DCs interacting as they travel through the LN. T cells display rapid motion in LNs, moving at an average of 10-12 $\mu\text{m}/\text{min}$ and a peak velocity of 25 $\mu\text{m}/\text{min}$. On the smallest time scale, the motion varies linearly with time, having a mean free path $\approx 30 \mu\text{m}$ and changing path direction on average every 3 minutes (57). Over longer time scales (up to 20 minutes) displacement-squared varies almost linearly versus time, characteristic of a random walk and quantified by the motility coefficient $\approx 65 \mu\text{m}^2/\text{min}$ (58). Since T cells must traverse a LN in <48 hours (as observed in classical studies of lymph circulation, ref. 59) their motion must be biased toward migration from entry at the afferent lymph to exit at the efferent lymph over the time scale of hours to days. Alternatively, if the motion through the LN conformed to a random walk with a motility coefficient of $65 \mu\text{m}^2/\text{min}$, T cell migration through the LN would take 24 hours to move 600 μm from the starting point and more than 10 days, on average, to be displaced 2 mm. Both of these distances would represent unrealistically slow movement through the LN, particularly since the T-cell motility decreases when bound to a DC or when the T-cell enters the medullary sinuses on the path to exit from the LN via the efferent lymphatic. (Note these calculations do not refer to the total path length but rather the net displacement from the starting point for a completely random walk.) Once a T cell binds to a DC with cognate antigen, its movement slows with binding lasting over a period of 10-15 hours; clusters of T cells form around the DC followed by swarming behavior of the T cells (60). Following this prolonged contact, both T cells and DC are activated (a fully activated DC is known as a licensed DC, or LDC), and T cell proliferation begins (60).

Unfortunately the processes captured via intravital microscopy technique represent very short time scales (minutes to hours) and occur over very small length scales (100 μm). Intravital microscopy therefore captures a relatively small region of an entire LN, which can be larger than 1 cm^3 (and during infection grows even larger) and over a relatively brief time slice of an adaptive immune response that occurs over days to weeks. Further, simultaneous assessment of the processes occurring at different biological scales and time scales cannot be made by microscopy studies at this point. Image analysis is also time-consuming and complicated (55). As a result many details regarding human LNs and the role these structures play in determining the outcome of the immune response remain to be elucidated (43).

The anatomy of the LN is important in discerning not only antigen presentation events but requirements for trafficking into and out of the node. The structure and composition of HEVs determine T cell entry into the LN (43, 61). During inflammation cells that would normally exit from the LN might be blocked (62), leading to a sudden increase in cell numbers within the LN. While T cells enter through HEVs, DCs enter through the afferent lymphatics. After entry DCs position themselves around HEVs (63, 64), allowing for efficient scanning by T cells immediately upon entry. Thus the dynamic processes of trafficking into and out of the LN can greatly enhance the opportunity for antigen presentation to occur as well as determine its success (65).

Circulation of immune cells between blood and other physiological compartments

Ultimately the success of the initiated immune response also depends on the ability of APCs to traffic to LNs and the ability of activated T cells to return to the site of infection, events dependent on input from multiple compartments including both the blood and lymphatic systems. Of the more than 10^{11} immune system cells in constant circulation between the blood and lymphatics, only a small proportion (10%) of activated cells travel to the LNs on a regular basis. The other 90% circulate to the spleen, lung, liver, bone marrow, and other parts of the lymphatic system (66, 67). The purpose of this trafficking is to maintain immune surveillance in all parts of the body so as to rapidly mobilize cells to sites of antigen challenge (68). For example, to understand the dynamics of infection with *Mycobacterium tuberculosis* (*Mtb*), one would need to consider the flow of immune cells between the LN and the lung (69, 70). The entire process of T cell trafficking through lymph nodes occurs over a 24-48 hour time frame with T cells spending the majority of their time in the lymphatics (71, 72). This circulation is critical for driving LN dynamics.

Trafficking of DCs from the site of infection where they encounter and take up antigen to the closest draining LN is the first step in the cascade of events leading to adaptive immunity. DCs must migrate from peripheral sites into the paracortical regions of the LNs to optimally encounter T cells (65). During the course of migrating from the site of infection to the LN, DCs undergo a number of changes collectively referred to as maturation. These changes include a cessation of the rapid pinocytic rates DCs display at peripheral sites and an increase in MHC class II expression. Upon reaching the LN, DCs carrying antigen are classified as mature. Although data support the presence of immature DCs in the LN, it is unclear how they come to be there. Immature DCs either must migrate in or are generated from monocyte precursors in the LN. Naïve T cells are constantly circulating through the lymphatic system to encounter antigen presented on DCs. The adhesion molecule L-selectin (CD62L), expressed on naive $CD4^+$ T cells, is essential for entry of cells into the LN (73). The process of T cells circulating to the LNs in this fashion is referred to as homing (73). Effector T cells that have been primed in the LN must circulate back to the site of infection to participate in the clearance of the pathogen.

Pathogens regularly interfere with antigen presentation

Pathogens regularly interfere with immune processes (74). Since pathogens meet APCs continually as a first line of defense, it should not be surprising that viral and bacterial pathogens have evolved ways to inhibit multiple aspects of antigen presentation both directly and indirectly. Cytomegalovirus is a viral pathogen that has been shown to inhibit antigen presentation by interrupting the MHC II expression pathway (75). Recently both Ebola and Hanta viruses have also been shown to interfere with antigen presentation (76).

An example of a bacterial pathogen that inhibits antigen presentation is *M. tuberculosis*. *Mtb* is the number one cause of death due to infectious disease in the world today (2 billion people infected). Upon entering the lungs *Mtb* is taken up by resident macrophages or DCs, adapts to the intraphagosomal environment, and either becomes dormant or slowly replicates (77). *Mtb* is known to inhibit antigen presentation in chronically infected macrophages. The mechanisms by which *Mtb* achieves this inhibition have not been completely elucidated, though several hypotheses have been proposed (cf. 78, 79, 80). Mathematical modeling is a tool that can be used to explore the mechanisms by which pathogens inhibit antigen presentation.

Approximately 14 million people have died in the AIDS pandemic. Over 40 million people are estimated to be HIV-positive, with about 4.9 million newly infected per year 81. Despite the impressive amount of research on HIV pathogenicity and immunology, there is no effective vaccine or cure. Ultimately, our capacity to fully treat or immunize against HIV is limited by our incomplete knowledge of the mechanisms behind the immune response to HIV-1, the more prevalent and virulent type of the virus. Since HIV-1 uses the CD4 receptor on the surface of both T cells and macrophages for entry and infection, these important immune cells are greatly affected. Specifically, the numbers and functionality of these important immune cell classes diminish during infection, eventually leading to AIDS. Although HIV-1 is not known to directly inhibit MHC II presentation, it disrupts many of the important events that occur both upstream and downstream of T cell recognition of pMHC complexes. A comprehensive model of antigen presentation encompassing adaptive immunity would allow for a greater understanding of how the immune response fails in HIV-1 and highlight targets for therapeutic intervention.

Antigen presentation as a multi-scale process

Processes at several length and time scales govern antigen presentation and the development of an immune response as summarized in *Table 1A*. The binding affinity of MHC II and peptide depends not only on the peptide sequence but also on the particular MHC II allele. Peptide-MHC binding is a molecular-scale event that is embedded in the context of single cell-scale events, e.g. antigen uptake, MHC synthesis, antigen processing, and pMHC trafficking and display, which occur on a time scale of minutes to hours. In the LN environment, a tissue space of $\approx 1 \text{ cm}^3$, T cells meet APCs and over a period of hours to days cells interact with APCs, divide, migrate through the LN, and exit. Finally, at the organ/organism scale, exiting cells go to sites of infection to

participate in the adaptive immune response which bears a length scale that encompasses the entire organism and a time scale of days to weeks.

<i>Biological</i>	A: Scale		B: Modeling	
	<i>Time</i>	<i>Length</i>	<i>Dynamics</i>	<i>Model Type</i>
Molecular	10^1 - 10^2 s	10^{-9} - 10^{-8} m	Deterministic, continuous	Statistical
Cellular	10^1 - 10^3 s	10^{-5} m	Deterministic, continuous	Mathematical: ODE
Tissue	10^4 - 10^5 s	10^{-3} - 10^{-2} m	Stochastic, discrete	Algorithmic: ABM
Organ/ organism	10^5 - 10^6 s	10^{-2} -1 m	Deterministic	Hybrid: ODE+ABM

Table 1. Relevant scales and features associated with the different antigen presentation events. (A) Biological events occur at different time and length scales. (B) Modeling approaches described here. ODE = ordinary differential equations; ABM = agent-based model.

Of primary interest is the entire multi-scale system: the immune response and the outcome of infection in a host. How this complex system depends on various parameters and even therapeutic manipulations at the different scales is a key goal. Yet given its complexity the entire multi-scale system is presently impossible to study in an experimental setting. Thus we turn instead to building a multi-scale model of antigen presentation and its role in the immune response.

Certainly there has been a wealth of basic science performed at the various biological scales attempting to elucidate these processes. Indeed, events at each scale of the antigen presentation process are likely to affect the overall development of the immune response. Thus models built to elaborate the relevant interactions and dynamics at each of the individual scales are the first step towards understanding a larger picture. Ultimately the integration of such models will provide a multi-scale model of the process.

Such a multi-scale approach will allow us to address questions that bridge biological scales. For example, can particular MHC alleles (molecular scale) give rise to more pMHCs on the APC cell surface (cellular scale)? Can higher pMHC affinity (molecular scale) compensate for poorer APC uptake ability (cellular scale) or fewer APC or fewer

highly specific T cells (tissue scale)? Could reduced display of pMHC by an APC (cellular scale) be compensated for by a longer residence time in the LN (tissue scale)? Will slowed cell circulation through the LN (tissue scale) slow or diminish the magnitude of the overall response (organ/organism scale)?

At the scale of an entire organism, a multi-scale model can address issues related to infection sites and other organ involvement. For example, how large must variations in the affinities of peptides for MHC (molecular scale) be in order to significantly impact the response (organism scale), and can such variation in affinities offer a basis for disease association? Multi-scale models are essential to reveal features that cannot be predicted by a focus on a single spatial or time scale. To begin to address these issues, we now present efforts made using modeling approaches at each of the scales and discuss how we might link these individual models to generate a multi-scale model of antigen presentation.

Modeling approaches

Models at individual scales

It would be difficult to imagine a single experiment that could shed information on all the different spatial and time scales involved in antigen presentation. Similarly, constructing and validating a model encompassing all of these events presents unique challenges. The approach we describe below is to build models at each of the different scales and then develop methods to link them together. For each of the biological scales represented in *Fig. 1*, different statistical, mathematical, or algorithmic models have been developed (*Table 1B*).

At each scale a decision needs to be made regarding the appropriate type of model to construct. Statistical models can be used for uncovering trends when large data sets are available. Here an understanding of mechanisms is not necessary; rather, mechanisms may be inferred from the results of the analysis. Mathematical models involve equations to describe biological events, and these may be solved analytically or numerically. Algorithmic models are implemented on the computer as a detailed sequence of rules. Hybrid models are also possible. Several excellent texts are available that describe the use of each of these models in biology, particularly mathematical models (82, 83, 84, 85, 86, 87, 88). A limited number of texts are also available describing the biological applications of statistical models (89-91) as well as algorithmic models (86, 92).

Models may be categorized in one of several ways. First, models may be continuous or discrete. Continuous models treat entities not as individuals but as an averaged population or concentration; e.g. the concentration of a cytokine might vary continuously from 1 nM to 5 nM within a LN. Discrete models treat entities as individuals; e.g. a single cell could be tracked as it moves through a LN. Secondly, models may be stochastic or deterministic. Stochastic models have random events that affect the outcome; e.g. a cell may move to the right or to the left with equal probability. Each individual simulation will give a slightly different result. The results of multiple

simulations can be averaged and standard errors obtained. Deterministic models, on the other hand, yield the same result each time they are solved or simulated, capturing for example an average behavior of a molecular or cell population rather than particular outcomes.

Ultimately the choice of modeling approach depends on considerations of the biological scale of interest—its spatial and time scales, the questions to be posed, whether tracking individual entities is important, etc.—as well as practical considerations such as available computing resources. In some cases new insights may be found by using multiple approaches to a single problem (93).

Parameter estimation and sensitivity analysis

A critical issue to all models at any spatial or time scale is that of estimating parameter values (e.g. rate constants, concentrations, probabilities of a particular event, etc.). There are several approaches possible for estimating parameter values: (a) direct experimental determination of a parameter, (b) simultaneous estimation of several parameters at once by fitting experimental data to a model (e.g. 94), and (c) estimation of a parameter based on known values for similar systems. In all cases there is necessarily some uncertainty in the parameter value (due, for example, to experimental error, differences in animal models, and technical limitations in kinetic measurements), and this leads to uncertainty in the output of any model using that parameter.

Because our models include parameters describing a large number of known biological processes, it is critical to understand the role that each of these parameters plays in determining output. Sensitivity analysis involves the correlation of variances in parameter values to variances in model output and is particularly useful when parameter values are not known with certainty. If simulations can be performed relatively quickly, all parameters can be varied simultaneously to ascertain those that contribute to significant variations in output variables. In the Latin hypercube sampling (LHS) algorithm each parameter is assigned a distribution, typically uniform or normal and centered on a baseline or estimated value, allowing the effect of under- and over-estimation to be examined. The entire range of each distribution is then sampled to generate a set of values for each parameter, and parameter values for each simulation are chosen to cover the entire parameter space in as few simulations as possible (95, 96). Although originally developed for differential equation models, we have recently adapted the algorithm for use in other types of models (97, 98). The extent to which each parameter affects the output can be quantified by one of several metrics including the partial rank correlation coefficient (PRCC). PRCC, like the more familiar Pearson correlation coefficient, varies between -1 and 1 indicating strongly negative and positive associations, respectively. A PRCC of 0 indicates no association. PRCC values can also be calculated at different time points of the simulation allowing the relative importance of a particular parameter in determining model output to be tracked over time. In addition a confidence interval can be determined for each PRCC, and differences between PRCCs can be tested for statistical significance (99). This allows parameters to be ranked in order of effect on output by PRCC magnitude.

The results of sensitivity analysis can be used to identify which interactions or processes in a system are important to different observed behaviors, i.e. which of several processes dominates at a particular time. In addition the results can be used to identify potential targets for therapeutic intervention; e.g., one could target a pathway to which cell behavior is sensitive as identified by sensitivity analysis.

Models

Here we present four different models developed to capture antigen presentation processes at the four different biological scales shown in *Fig. 1*. (See *Table 1B*.)

Algorithms for predicting peptide-MHC binding affinities

Peptide-MHC binding is a prerequisite for antigen presentation and the event most likely to be affected by polymorphisms that exist within the MHC of human populations. From a clinical perspective these polymorphisms may distinguish individuals who succumb to a particular infectious disease from those who remain healthy, and significant effort has been expended to assess whether binding occurs between relevant peptide-MHC combinations. However, the sheer numbers of possible peptides (20^9 or $\sim 10^{11}$ peptides of length nine) and MHC molecules (more than 2200 known HLA alleles) make this task all but impossible for anything more than a small sampling of the peptide-MHC combination space.

To circumvent this difficulty computational algorithms have been developed to predict whether binding occurs between particular combinations of peptide and MHC (*Fig. 4A*). In general these algorithms have the same aim as other algorithms in bioinformatics: to identify patterns in sequences that are known to either possess or not possess a particular trait. In this case the trait is binding to a particular MHC molecule.

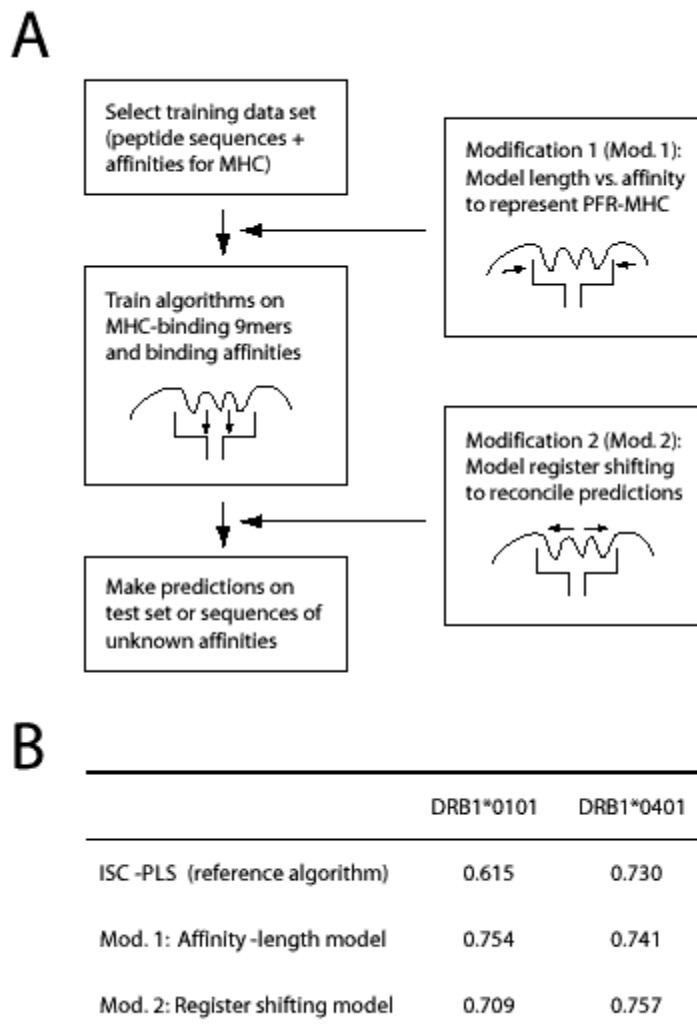


Figure 4

With this aim in mind computational algorithms have been built around a number of statistical and machine learning methods to predict peptide-MHC binding (*Fig. 4A*). The first and simplest algorithms were based on the identification of motifs within peptides binding particular MHC (100). An example of such a motif is the requirement for a hydrophobic amino acid at the N-terminus (position 1) of a 9mer binding MHC of the DR1 serotype, a guideline still generally followed today (16). The advent of competitive binding assays allowed a more nuanced view of binding to be taken. Motifs that required certain amino acids to be present in MHC-binding peptides were superseded by matrices scoring amino acids at each position within the peptide. Different statistical methods could be used to generate the elements of the matrix, including nonlinear and linear programming (101, 102), stepwise discriminant analysis (103, 104, 105), and partial least squares (106, 107). One simplifying assumption made in many of these algorithms is that

binding of each amino acid within the peptide to the MHC molecule occurs independently of adjacent as well as more distal amino acids. Though this assumption was largely confirmed by available crystal structures, algorithms were also developed that did not rely on this assumption based on machine learning methods. Several machine learning methods have now been incorporated into prediction algorithms including artificial neural networks (108, 109, 110), hidden Markov models (111), and support vector machines (112, 113).

A different approach has been to predict the structure of the peptide-MHC complex and attempt to calculate the free energy change (114, 115, 116, 117, 118). Structure-based prediction may someday supplant statistical- or machine learning-based algorithms but is currently hampered by the limited availability of solved structures and high computational costs. For a more comprehensive review of algorithms, the reader is referred elsewhere (119, 120).

An obvious question to ask about the preceding list of algorithms is how well each one performs compared to the others. To gauge prediction accuracy an algorithm that has been trained on a set of data is used to make predictions on a test data set for which affinities are known, and the output of the algorithm is compared to the known affinities (*Fig. 4A*). A score is then calculated to determine how closely predicted affinities approximate known affinities; however, this task is complicated by differences in the nature of algorithm output. In some cases output is a continuous variable (affinity), while in other cases discrete (binding or non-binding). This reflects differences in the nature of the available binding data on which these algorithms are fitted or trained. Some databases provide only lists of peptides that either bind or do not bind particular MHC variants (121) while other databases provide a measure of affinity such as IC_{50} (20). The appropriate performance measure therefore differs according to whether input and output are both continuous (Pearson correlation coefficient), both discrete (Matthews correlation coefficient), or discrete and continuous, respectively (area under receiver operating characteristic curve, or A_{ROC}). The A_{ROC} plots represent the probability of true positives vs. false positives, given a particular threshold or cut-point for a discriminatory test. A completely random outcome would have an area = 0.5, while a test that perfectly discriminates (detects all true positives and no false positives) would have an area = 1.0. As with PRCC these correlation coefficients vary between -1 and 1 while A_{ROC} ranges from 0.5 to 1.0. In both cases higher scores indicate more accurate predictions. Continuous data can be converted into discrete data by assuming that a certain threshold affinity is required for binding such as an IC_{50} of 500 nM (21) allowing some overlap between performance measures. Examples of scores obtained for several algorithms are provided in MHCbench (122). For example, using binding data for the human MHC II allele HLA-DRB1*0401 from which homologous sequences had been removed, twelve algorithms were found to produce A_{ROC} scores between 0.57 and 0.76.

Our efforts in this area have focused on improving how prediction algorithms handle features that distinguish MHC II-binding peptides from MHC I-binding peptides. Because peptides binding MHC I lack the heterogeneity in peptide length characterizing MHC II-binding peptides, most prediction algorithms were originally developed in the

context of MHC I. Adapting these algorithms to MHC II therefore requires an assumption to be made regarding how heterogeneity in length affects binding. One possibility is that parts of the peptide extending past the ends of the MHC II peptide-binding groove, the so-called peptide flanking regions (PFR), interact with more distal areas of the MHC molecule (123). In most algorithms it is assumed that PFR do not interact with the MHC molecule and have a negligible effect on binding. In addition, longer peptides are also more likely to have additional binding registers (9mer subsequences that fit in the binding groove) allowing shifting among the registers. Some algorithms assume that the highest affinity register predominates (18, 124). Other algorithms assume that all registers are presented in equal numbers and predict the measured binding affinity to be the mean affinity of the different registers (107). We have proposed instead that registers are presented in quantities proportional to their equilibrium affinities and that the measured affinity of a given peptide-MHC complex therefore represents a weighted average (Chang *et al.*, submitted), a situation analogous to competition between receptors of different affinities for ligand (87).

We hypothesized that the effects of PFR interactions and register shifting could be discernible in plots of affinity versus length and could be taken into account either by filtering the data prior to use in algorithm fitting or training (in the case of PFR-MHC interactions) or by using an equation for register shifting (*Fig. 4A*). Recently we have shown that both modifications significantly improve the performance of multiple algorithms (Chang *et al.*, submitted). In *Fig. 4B*, the results of our modifications for one such algorithm, ISC-PLS (107), applied to two MHC alleles are shown. These results are consistent with past experimental studies showing that peptide length affects binding to a number of MHC alleles (125, 126).

In sum the output of these computational algorithms is a prediction of binding between particular peptides and MHC alleles, one measure of which is the equilibrium dissociation constant of a peptide-MHC complex (K_D) or the related IC_{50} . (In the remainder of this review, we use the term affinity to refer to the reciprocal of K_D so that higher affinity refers to stronger binding.) Affinity is one of several parameters that determine the number of pMHC displayed on the surface of the APC. To understand the role that cellular parameters also play in determining pMHC display, we next turn to models of the APC.

Models for antigen processing and presentation by APCs

Peptide-MHC binding is only one step of many that constitute the antigen presentation pathway, and other steps may confer additional specificity to or alter the dynamics of which peptides are ultimately presented (see *Fig. 2*). In both MHC I- and MHC II-mediated antigen presentation, antigens are acquired (from either an intracellular or an extracellular source), degraded into peptides (i.e. processed), and trafficked to the cell surface after binding MHC. At the same time MHC molecules are synthesized, trafficked to and from the surface, and degraded. Many of these steps are subject to complex regulation by the cytokine environment and feedback signals. The peptides found to bind

a particular MHC variant may therefore only provide a rough, static approximation of peptides that are ultimately presented in a dynamic fashion.

Models of antigen presentation must therefore account for more than peptide-MHC binding. In the case of MHC I-mediated antigen presentation, at least two additional events are known to confer selectivity: proteasomal cleavage and TAP transport. Algorithms have been developed to predict which peptides progress through these stages, and only recently have they been daisy-chained together with algorithms of peptide-MHC binding to represent antigen presentation *in toto* (127, 128). The result is a more accurate but still static picture of the peptides encountered by CD8⁺ T cells.

In contrast we were initially interested in the dynamics of MHC II-mediated antigen presentation but not necessarily its specificity. To track the levels of different molecular intermediates in the pathway we used a mathematical representation known as ordinary differential equations (ODEs). ODEs are commonly used to represent systems that are both continuous and deterministic. One assumption made in using ODEs is that the represented entities exist as large, well-mixed populations (i.e. can be approximated as continuous). For MHC II-mediated antigen presentation the available data validated this assumption. Baseline estimates of the number of MHC II molecules expressed by APCs were on the order of 10^5 and antigen was typically present at high concentrations, at least *in vitro* ($>10^{12}$ peptides per cell 79, 80). Furthermore precedent for using ODEs had been provided by models of receptor-ligand systems of which peptide-MHC could be considered one instance (87).

Using a series of models that have incorporated increasing amounts of biological detail, we have been able to address different aspects of antigen presentation that have not always been tractable in the laboratory setting. The first model included only those intracellular processes thought to be essential to antigen presentation (antigen uptake and processing, peptide-MHC binding, and MHC trafficking and recycling) but was sufficient to generate realistic time courses of peptide-MHC levels on the APC surface of both macrophages and B cells (129). Parameters that would have been difficult to manipulate experimentally, e.g. the rate of antigen uptake, were easily varied in the model. The relationship between these parameters and the level of antigen presentation could then be studied without concerns of inhibitor toxicity, etc. Later versions of this model included self peptides and TCR and expanded the range of questions that could be asked, including: At what density are exogenous peptides presented relative to self peptides (130), and can higher peptide-MHC affinity offset lower pMHC-TCR affinity to engage the same number of TCRs (41)?

In the latest version of this model we have included the regulatory effects of IFN- γ to more closely mirror experimental protocols used *in vitro* (131, Fig. 2). For parameters that were unique to this model, values were either derived from the recent literature or constrained by biological requirements (e.g. to maintain low-level MHC expression in resting APCs, as observed experimentally). The model was tested by comparing the dynamics of several output variables to experimental data. For example, times at which CIITA mRNA and MHC II mRNA reached maximal levels following IFN- γ stimulation

were compared in simulation and experiment and found to be similar (*Fig. 5A, B*). The final model contained 16 variables, each representing a different molecular species, and 30 rates or rate constants.

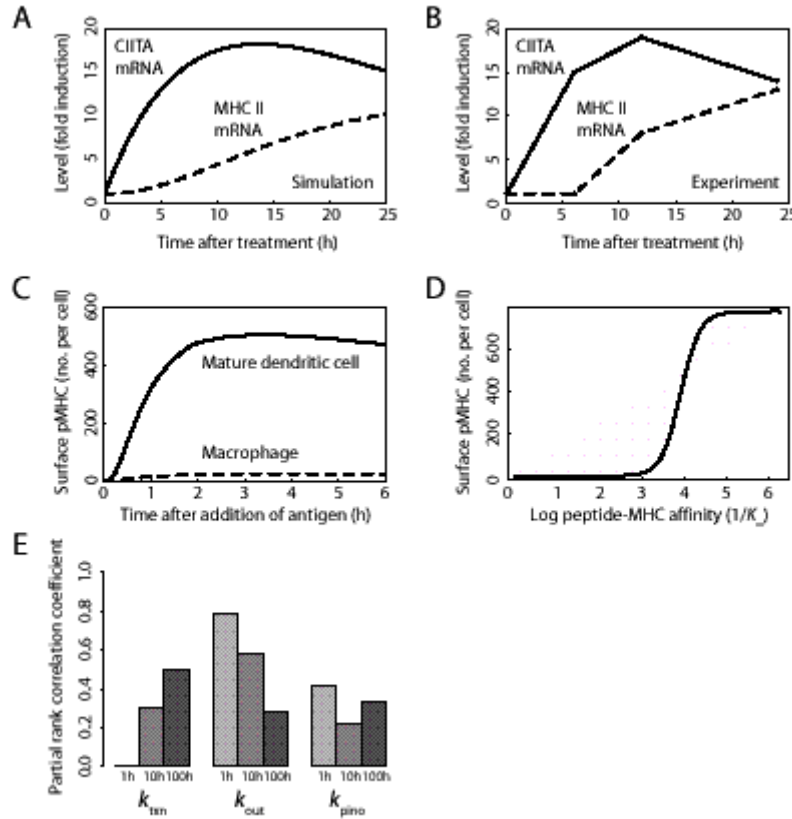


Figure 5

This model was developed initially to explore presentation dynamics in macrophages. However, with appropriate parameter values it can be used to simulate pMHC display by DCs as well. Because DCs have an enhanced capability for antigen uptake and greater numbers of MHC available (132, 133), they display more pMHC on their surfaces than macrophages (*Fig. 5C*).

There were several key findings of our model. First, the number of cell surface pMHC was calculated and shown to be a strong function of a molecular scale parameter, peptide-MHC affinity (*Fig. 5D*). This is relevant to the linking of individual models (here, molecular and cellular scales) to produce a multi-scale representation of antigen presentation. Second, sensitivity analysis revealed that particular cellular parameters may have increasing or decreasing effects on pMHC levels over time (*Fig. 5E*). For example,

the effects of varying rates of MHC transcription are only apparent at longer time scales (here, 10-100 hours) while the effects of varying trafficking of pMHC to the cell surface plays a more prominent role early in the process (1 hour), showing how the importance of a particular intracellular process to surface pMHC levels can be time-dependent.

Models of cell-cell interactions in the LN

Up to this point our focus has been on molecular and cellular events involved in antigen presentation. Here we examine the interactions between cells of the immune system and place these dynamics in the context of the environment that houses the majority of antigen presentation activities: the LN. This not only allows us to bring another key biological scale into our model—that of tissue—but also brings us closer to the goal of developing a full-system model of antigen presentation and its role in the immune response.

There have been numerous mathematical models studying the interactions of immune cells (for a review, see 134). Most of these earlier models of cellular dynamics were built on ODE systems that were continuous and deterministic in their abstraction of cellular events. Typically the LN is not explicitly included; however, when it is considered, it is treated as a coarse-grained (i.e. with little mechanistic detail), well-mixed compartment and the spatial structure is disregarded.

We recently explored the dynamics of antigen presentation within the LN using an agent-based model (ABM) approach (Bajaria *et al.*, submitted). ABMs are algorithm- or rule-based models that allow for a discrete and stochastic representation of cells and events (86). In an ABM cells (or any other entity of interest) are represented as discrete software objects (or “agents”) and placed on a lattice. Rules are assigned to the agents governing their movement and interactions within the lattice that represents the LN in our model. A time step is then specified for the model based on considerations of durations of cell movements and interactions (e.g. 1 minute to move one cell length), and the model is run for as many time steps as desired. ABMs therefore have the following components in common: (1) agents, (2) the environment where agents reside, (3) the rules that govern the dynamics of the agents, and (4) the time scales on which these rules are executed. We describe each of these components as they are represented in our model below.

The goal of our model was to understand how the interactions of individual APCs and T cells within the specific spatial and chemical environment of the LN generate observed numbers of activated T cells. An ABM is useful here as it allows tracking of individual APCs and their interactions with both T cells and their environment. ABMs can capture spatial aspects of the system as well, for example the particular geometry of the LN and any groupings of cells that develop. These features are not readily available in the more commonly used differential equation formulations. Another advantage of ABM over ODE model representations is the opportunity to observe how outcomes are influenced by various stochastic events that are not wholly deterministic. We do note, however, that a disadvantage of ABMs as a model framework at this early stage in their development is a shortage of rigorous analysis techniques; models tend to be highly specific and

parameter-dependent. Furthermore, because stochastic events influence the outcome, a large number of simulations are required to characterize the mean behavior of the system. In a recent study by our group, we compared four different modeling techniques to explore a different immunological problem—how a granuloma (a spheroid mass of APCs, T cells, and bacteria) forms during TB infection—and while each of the approaches made important and consistent predictions, the ABM yielded the most realistic results (135).

The agents in our model are the cells known to participate in antigen presentation events. In our initial studies we have included $CD4^+$ and $CD8^+$ T cells and DCs. Because this model captures only a single LN, we used phenomenological source functions describing the entry of cells to the LN. We count cells as they exit the LN as well but do not track them further.

The spatial environment of our model consists of a two-dimensional (2-D) lattice with 100 microcompartments, each of size $20\ \mu\text{m} \times 20\ \mu\text{m}$ and together large enough to represent a single human LN (see *Fig. 3*). T cells and DCs interact in the LN paracortex, a region facilitating communication between immune mediators such as cytokines and the cells that they influence (56). Each microcompartment is designed to hold only one DC, the largest cell in the system. Up to two T cells can share the same microcompartment, and multiple molecules (e.g. cytokines and antigen) can also be found in each microcompartment. A 2-D representation is reasonable for ease of computation. Also, analysis of multi-photon microscopy data from 2-D cross-sections indicates that the majority of dynamic behavior occurs in the 2-D plane and only occasionally do cells jump to other depths (out of the plane of observation) (M. Miller, personal communication, and 57).

Also included as part of the environment are antigens (whether non-specific or from a particular bacterium or virus) and cytokines/chemokines such as IL-2. These are all treated as continuous variables that are real-valued in each microcompartment of the lattice. Treating molecules in solution as continuous variables is reasonable as the concentrations of these molecules are high in comparison to cell numbers.

Discrete agents in the model are assigned a set of states and rules. As an example, a $CD4^+$ T cell can have one of four states: resting (and naïve), activated or effector. They also have a lifespan. For each state, rules are specified governing the interactions possible for that state. One such rule is the following (see *Fig. 6*): If a mature DC (MDC) encounters and binds a resting $CD4^+$ T cell in one of 8 neighboring microcompartments for 15 hours (136) then the $CD4^+$ T cell becomes activated with probability p . (Note- since two T cells can occupy one microcompartment, this means that a single DC can bind up to 16 T cells at one time). For each implementation of the rule, a number is drawn from a uniform distribution with range $[0, 1]$ and when the chosen number is less than the parameter value, e.g. $p = 0.25$, then the event occurs; otherwise, it does not. (This again illustrates the contrast between a deterministic vs. ABM implementation of a probability rule.) Predictions using different probabilities of activation can be generated, and the effect on the system can be examined using sensitivity analysis. Other rules account for the ability

of DC dendrites to scan neighboring compartments for cognate T cells, allow a resting T cell to remain bound to a DC for 10-15 hours while becoming activated, and allow a mature DC to bind up to 16 T cells, as observed in microscopy studies (68, 60). The rules for APC-T cell interactions in this model are flexible and can accommodate many different lines of experimental evidence regarding how these cells interact. The time step used for updating cell position was 2 minutes. Other time-dependent phenomena included lifespan of cells, duration of cell binding, and recruitment of new T-cells via the HEV.

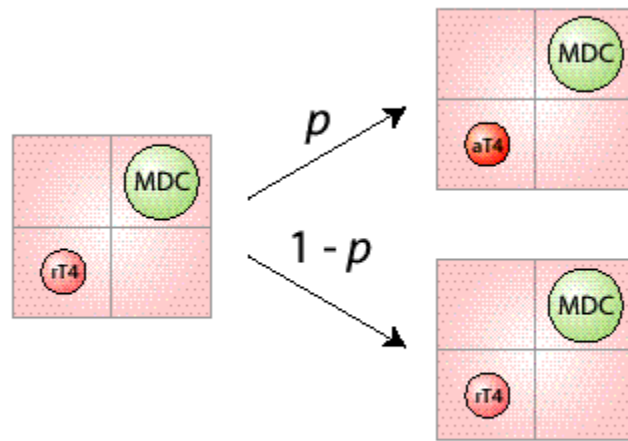
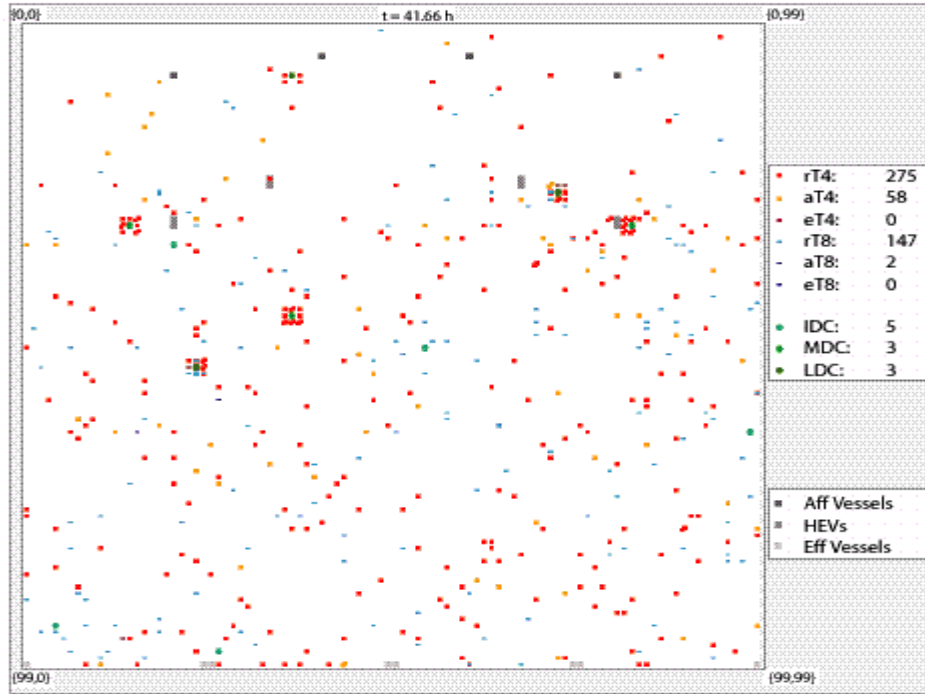


Figure 6

Simulations of a number of different conditions were performed. The negative control depicts simulations in the absence of antigen. In this case immature DCs and resting $CD4^+$ T cells are present in homeostatic numbers (data not shown). *Fig. 7A* shows T cells and DCs in the LN at a single time point (approximately 42 hours) of the simulation after the arrival of six MDCs from a site of infection. What is evident for the first time using our model is a spatial organization to the dynamics of antigen presentation. For example, in *Fig. 7A* clusters of DCs and T cells are seen. Such clusters are necessary for activation of T cells as well as licensing of mature DCs (60). As in the microscopy we observe that these clusters move and conjoin (M. Miller, personal communication).

A



B

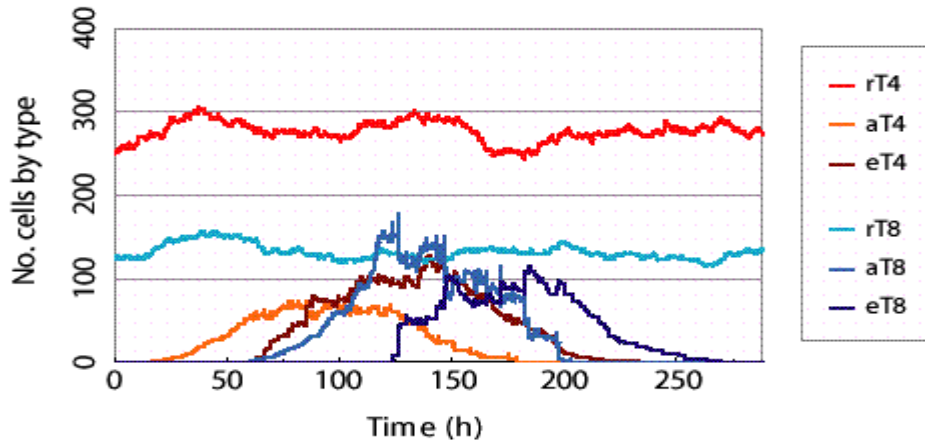


Figure 7

To track the total sizes of the cell populations as they evolve over time, snapshots such as that shown in *Fig. 7A* are enumerated for each cell type. *Fig. 7B* shows the temporal dynamics of each of the cell populations over the entire time frame of the simulation and indicates the following course of events for T cell dynamics over the simulated infection. With the introduction of only 6 mature, antigen-bearing DCs on day 0 (into a system that is already in homeostasis), we see an increase in activated $CD4^+$ T cells (aT4) and then a day or so later a similar increase in effector $CD4^+$ T cells (eT4). Effector $CD4^+$ T cell numbers peak at ~6 days (~140 hours), 2 days after activated $CD4^+$ T cell numbers peak. Both decline slowly after that. This is expected as immature DCs have a lifespan in the

range of 1-9 days, MDCs have a lifespan of 3 days, while licensed DCs have a lifespan of 1.5 days. (In the model licensed DCs are MDCs that have engaged a CD4⁺ T cell for a long period of time or after having engaged an effector CD4⁺ T cell.) No additional mature DCs were introduced in this simulation. CD8⁺ T cell numbers follow a similar path, and in addition memory cells are generated. Notice that the levels of resting CD4⁺ and CD8⁺ T cells remain in homeostasis even during this infection scenario. This result emerges from the model and represents a natural feedback regulation that occurs. Thus while cells are being recruited to the other subclasses (i.e. through activation), new cells continue to enter into the LN to replace them, maintaining homeostatic resting T cell numbers and supplying new T cells that can be recruited to an activated state.

To illustrate the usefulness of sensitivity analysis in this setting, we explore the parameter representing the probability that binding between a CD4⁺ T cell and its cognate MDC results in activation of the T cell. As discussed above, T cell activation likely depends on many factors including the number of pMHC on the surface of the DC as well as the binding affinity between pMHC and TCR. In our ABM these factors are combined into the representative parameter p . Fig. 8 shows a dynamic plot of two model outcomes, the number of activated CD4⁺ (panel A) and activated CD8⁺ T cells (panel B) in the LN versus p (the probability that a CD4⁺ T cell becomes activated upon encounter with an MDC or LDC) at four time points. In both cases activated CD4⁺ and CD8⁺ numbers increase as a function of p . Activation of both cell types is a strong function of p , and this could be explored further by integrating finer detail in this term (i.e. by incorporating the smaller length scale models described earlier); a first step at a multi-scale approach.

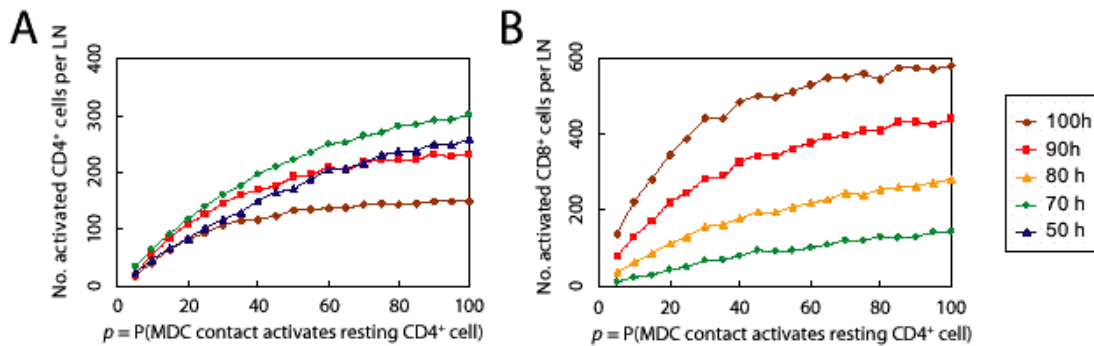


Figure 8

The ABM allowed us to obtain information regarding individual cell behavior for different cell types. This approach was in many ways superior to that of continuous models for the questions we were exploring here. First, we could track the location and state of all cells at any given time point allowing determination of spatial dynamics. Second, individual cell-cell interactions could be tracked in both space and time. These features allowed us to make predictions regarding biological mechanisms that were not feasible using continuous model approaches. For example, we determined that the

lifespan of licensed DCs greatly affects the number of effector CD8⁺ T cells generated (PRCC = 0.75 with p-value < 10⁻⁶). If a therapy could be identified to prolong licensed DC lifespan, then the model predicts a greater cytotoxic T cell response would be generated.

Finally, in the ABM of the LN we were able to track how many effector cells leave the LN over time. However, the model did not capture the trafficking events of these cells from the LN back to the site of infection, the next important step in the immune response. In addition the entry of cells into the LN was represented simply—using a single parameter—which does not account for factors such as the amount of antigen initially produced at the site of infection that ultimately limits the number of mature DCs. In the next section we discuss ways to integrate the LN into a more complete model of trafficking of cells during an immune response.

Multi-compartment models of the LN with other organ systems

In order to capture the full spectrum of immune system dynamics in a model, it will be necessary to include physiological compartments in addition to the LN. Immune cells regularly circulate through the blood, and because of ease of access blood data are the major diagnostic available to the physician. However, blood data provide only a snapshot of a system that also includes the lymphatics (which drain the tissues, typically key sources of antigen and DCs) and various organs and sites of infection.

In order to capture different physiological compartments, a model is usually developed for each compartment separately and then linked to the other models by representing the trafficking of shared elements between the compartments. Most typically the dynamics within each particular compartment as well as the trafficking between compartments are described with ODEs, though other possibilities exist. Which compartments are included in any particular model will depend on the types of infection being simulated and the questions being asked. For example, in studies of the immune response to *Mtb* it will be critical to include the lung compartment where granuloma formation occurs. Further, developing models that include these additional compartments will influence the LN model described above. In that model phenomenological source functions were used to describe the trafficking of cells into the LN. In addition we tracked the number of effector cells leaving the LN but did not allow them to continue to play a role in the immune response. Thus the goal now is to capture more mechanistically the dynamics of those compartments external to LNs. This will bring us one step closer to developing theories regarding overall immune activation as it depends on local antigen presentation events.

Many compartmental models of biological systems and the immune system have been developed (137, 85). Here we review two sets of compartmental models developed by our group, the first developed to study HIV-1 infection, the other to study infection with *Mtb*. We present here the non-infection states of these models (i.e. the negative controls) to demonstrate that we can understand the dynamics in healthy scenarios (*Fig. 9*). In both cases the LN is represented along with an additional compartment relevant for disease: the blood in the case of HIV and the lung in the case of TB.

Our blood-lymph circulation models (*Fig. 9A*) were developed first for the case of no infection to observe homeostasis and then in the context of infection, specifically with HIV-1 (138, 139, 140). In one work (140) we used ODEs to track CD4⁺ and CD8⁺ T cells and DCs circulating within and between the blood and lymph compartments. The model successfully captures known dynamics of these cell populations in their respective compartments. Dynamics of cell turnover and migration are the main features represented in this model. In the model CD4⁺ T cell counts are about 2×10^{11} in total lymph tissue and approximately 1×10^3 per μl of blood. This matches what has been observed in humans (141). The ratio of CD4⁺ T cells to CD8⁺ T cells found in the model is 2:1 in both blood and lymph, also as is observed (141, 142). We also predicted that there are 10^{11} CD8⁺ T cells in the lymph system and 5×10^2 CD8⁺ T cells per μl of blood, which agrees with data from Haase (141). The model also maintains a level of 14-20 DCs per ml of blood (143).

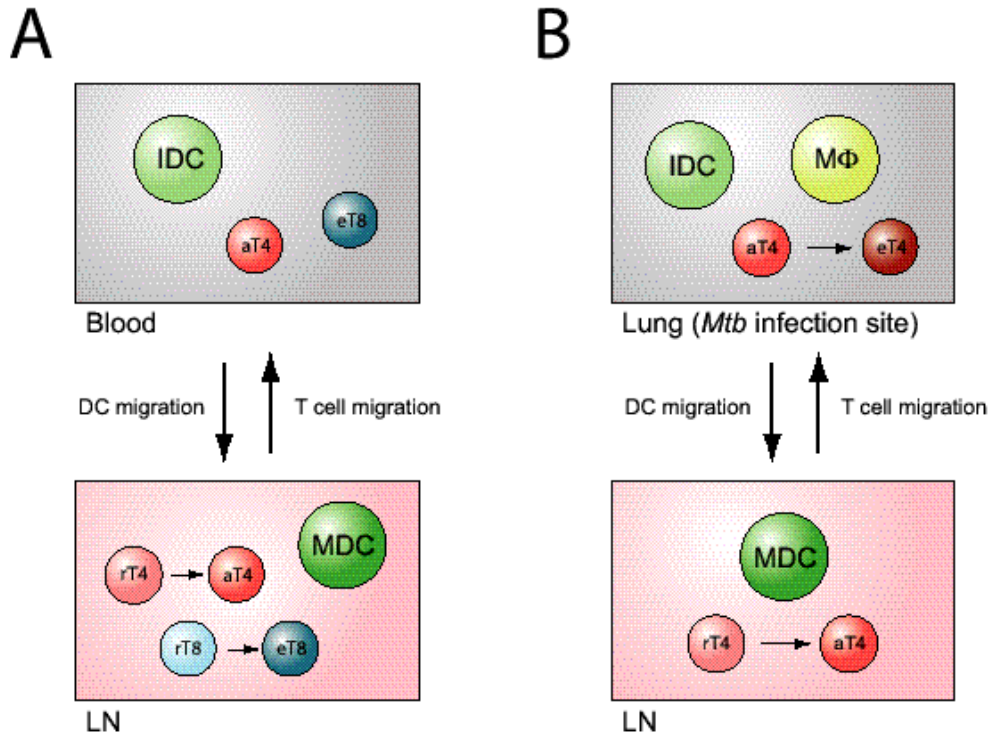


Figure 9

Our LN-lung compartmental model (*Fig. 9B*) is an example of a model that includes both the LN and an additional site of infection, the lung. Effector T cells generated in the LN via antigen presentation leave and travel to particular sites. For this model, which was developed with application to tuberculosis, the site of interest was the lung. The process by which effector T cells travel throughout the body is not well characterized and differs greatly depending on where the site of infection is located. The LNs that are typically involved are the closest draining LNs to the site of infection. This facilitates ease of trafficking between compartments.

As in the blood-lymph model, the simplest model here tracks only homeostasis of T cells and DCs between both compartments (69, 70). Specifically we linked a coarse-grain model of the LN based on a system of ODEs with an existing fine-grain ODE model (i.e. a model that includes many mechanistic details) of the immune response in the lung. In the lung model (144) we tracked resting, infected, and activated macrophages, Th0, Th1, and Th2 lymphocytes, the cytokines IFN- γ , IL-12, IL-4, and IL-10 and the level of antigen. Important in this model is the presence of macrophages playing multiple roles as APCs, cytokine producers, and killers of intracellular pathogens. In the coarse-grain LN we track mature DCs, resting T cells, Th0 cells and the concentration of the cytokine IL-12 (a promoter of Th1 immunity). In order to investigate DC trafficking, we modified the lung compartment by including immature DC in the lung model. In the absence of antigenic stimulation, i.e. at homeostasis, the LN compartment has an average of 10^4 naïve, resting CD4+ and CD8+ T cells, and all other cell types are absent. In the lung there are 5×10^4 immature DCs (approximately 10% of resting macrophage population) and all other cell types are absent. Our results are in agreement with lung and LN data from various animal models on the numbers of cells present in healthy subjects (145, 146, 147, 148, 149, 150, 151, 152, 153).

Applications of the individual models to study infection

Each of the individual scale models described above can be used to answer questions and suggest new experiments aimed at uncovering the roles that parameters (representing biological mechanisms) play in antigen presentation at each particular scale. Several examples are given below.

We used the model representing a single APC (*Fig. 2, Fig. 5*) to investigate why multiple mechanisms had been proposed to explain how *Mtb* inhibits antigen presentation in macrophages (131). For example, some researchers had identified MHC II transcription as a process which *Mtb* disrupts in macrophages. Others had suggested antigen processing or peptide-MHC co-localization as targets. By varying the rates or rate constants for particular processes in the model, we were able to predict the effect of the corresponding mechanisms on surface pMHC levels under different experimental conditions. We found that mechanisms could generally be categorized according to the timing of their effects. Targeting antigen processing or peptide-MHC co-localization, for instance, resulted in an immediate decrease in the ability of macrophages to present antigen, while mechanisms targeting MHC expression required a delay of at least 10 hours to become effective. However, the stimulatory effects of IFN- γ may necessitate the use of long-term mechanisms by a pathogen, particularly a slow-growing one such as *Mtb*. These two categories of mechanisms can therefore be thought of as non-redundant in function, suggesting that *Mtb* gains distinct benefits from inhibiting multiple intracellular processes.

Sensitivity analysis can be used to identify other possible mechanisms used by *Mtb* to inhibit antigen presentation. Because antigen presentation is required to resolve most infections, the results can often be applied to other pathogens as well. For example, surface pMHC levels were found to be sensitive to the rate constant for pMHC trafficking

to the surface at early time points (i.e. <10 hours post-infection, *Fig. 5E*). This process as well as others that have more significant effects early relative to cellular-scale events may make attractive targets for inhibition by pathogens with shorter doubling times. (Targeting transcription of MHC, in contrast, may require many hours to hinder antigen presentation.) This suggests one way in which antimicrobial therapies could be improved: ensuring that the pathogenic mechanisms targeted therapeutically are consistent with the time scale of the pathogen's lifetime.

Other examples of applying the individual-scale models build on our two-compartmental studies (*Fig. 9*). Our group and others have used multiple compartment models to study infection dynamics. The first models were developed to understand HIV-1 infection (154, 155, 156). Studies by our group looked in detail at the dynamics of circulation and trafficking of immune cells in blood and lymphatics during HIV-1 infection (138, 140). The latter model consists of a system of nonlinear ordinary differential equations that captures interactions between T cells and DCs and builds directly on the LN-blood model discussed above (*Fig. 9A*).

When HIV-1 is introduced into the system, additional cell types must be tracked. HIV-1 infects CD4⁺ T cells, so there is an additional class: infected cells. Further, because antigen is present, effector CD8⁺ and CD4⁺ T cells are generated in response to antigen presentation activities. Simulating this two-compartmental infection model yields good agreement with clinical data in both compartments. In the LN, resting CD4⁺ and CD8⁺ T cells both are estimated to be 10^{10} in number, while virus is 9×10^{10} and infected cells are 4×10^9 , similar to the results of 141. In the blood, activated CD8⁺ T cells are estimated to be 8.8% of total CD8⁺ T cells, which is in the same range as observed (157, 158). Our model predicts the ratio of activated to total CD4⁺ T cells in the blood to be approximately $1:10^8$, while the only available data suggest this ratio is roughly $1:10^3$. Our prediction varies depending on the level of interaction with DCs (for more details see 140). When the finer-grained models described above are linked with this model we should be able to better elaborate the mechanisms of CD4⁺ T cell decline during HIV-1 infection and better understand the role that antigen presentation plays.

We have also developed two-compartment models describing *Mtb* infection. Here we captured the dynamics of a specifically infected tissue (i.e. lung) and its closest associated LN, building on the LN-lung model discussed above (*Fig. 9B*; 69, 70). In addition to the variables included in the homeostasis lung model, we tracked both intracellular and extracellular load of *Mtb*. Once bacteria are present in the system, macrophages can take up bacteria at the site of infection and are classified as infected. If time passes and they are not activated sufficiently to clear their intracellular bacteria, then they are classified as chronically infected. Immature DCs that take up bacteria in the lung traffic to the LN to present antigen and generate effector cells that can now migrate back to the lung to participate in the adaptive immune response.

The model output qualitatively captures the main dynamics of a non-human primate infection model in both lung and LN compartments (see 69 and 70 for full details). The measured unit of the model is number of cells (or bacteria) per cm^3 of granulomatous

tissue. Total CD4⁺ T cell counts during latent TB in the mathematical model range between 1×10^3 - 1×10^4 (both in the lung and in the LN compartment). DC numbers during latent TB range in the lung between $2 - 2.5 \times 10^4$ in the mathematical model (a range similar to non-human primates). The main result of this work is that delays in either DC migration to the LN or T cell trafficking to the site of infection can alter the outcome of *Mtb* infection, defining progression to primary disease or latent infection and reactivated tuberculosis.

How to build a multi-scale model

Models developed at individual physiological scales can be linked to form a multi-scale model. Both mathematical/computational and biological issues bring complexity to this task; the development of efficient and computationally feasible multi-scale methods is an area of current investigation (7, 159, 160).

One of the simplest ways to link models is to have the output from one model be the input to another. Coveney and Fowler (161) and Vlachos (159) review an approach in which the results from a model developed at the smallest scale are passed to the model at the next scale, and so on, termed a hierarchical, sequential, or serial approach. For example, the output from a smaller-scale model may be the calculated value of an important parameter (e.g. affinity) or a set of values (e.g. the number of cells in a given state as a function of time). Even with a hierarchical approach, there are decisions to make. Does the larger-scale model contain the entire smaller-scale model? If so, then computation may be an issue. Further, with any numerical solver issues of error arise. For each of the individual models, numerical errors may accumulate, and the propagation of these errors by passing them across scales presents significant challenges.

Alternatively, if changes at larger scales affect behavior at smaller scales, for example if there is feedback occurring over multiple biological scales, a hierarchical approach is no longer valid (but may still be a useful starting point) and a hybrid or coupled multi-scale approach should be used. It is likely that this will nearly always be the case in biology. For example, changes in ion channels in the heart affect overall heart function. At the same time, blocking blood flow in a coronary artery also affects heart tissue at the cellular scale (162).

To begin to build a multi-scale model for our system of antigen presentation, we will need to interface the four individual-scale models under development and discussed above (summarized in *Table 2*) in a hierarchical fashion as shown schematically in *Fig. 10*. We work under the hypothesis that events at each scale (molecular, cellular, tissue, and organ/organism) of the immune system represented in a multi-scale model affect the development of the immune response. First, the output of our molecular-scale model, peptide-MHC II affinity, is a critical parameter that serves as an input into our single-APC model. This allows us, for example, to explore the effect that MHC II polymorphism may have on pMHC presentation (*Fig. 10A*). Second, the state of an APC agent, in particular the number of pMHC displayed on the surface as a function of time, can be calculated from our single-cell-scale APC model. At this point we can determine whether differences in peptide-MHC affinity found at the smaller scale give rise to

significant differences in pMHC display (*Fig. 10B*, cf. *Fig. 5D*). Third, the ODE simulations of the APC model will generate individual, single cell-scale information that will be used to update each agent within the tissue-scale model, the ABM of a single LN. In this model the number of pMHC complexes on the surface of an APC is currently represented as a probability p that an APC will activate a T cell with which it has come into contact, an input parameter for the ABM. We can now again determine whether differences in peptide-MHC affinity will play a key role, but this time by examining effector T cell numbers generated in the LN (*Fig. 10C*). Finally, we can use the fairly course-grained ODE models developed for particular, relevant body compartments (e.g. blood, sites of infection) together with the fine-grained agent-based LN model to see, for example, the impact of peptide-MHC affinity at the organism scale (*Fig. 10D, E*). One might compare the predictions of this multi-scale model with the data of Geluk *et al.* who showed that only a few TB-derived peptides elicit a T cell reaction in mice and that these peptides also bind MHC with high affinity (25). Similarly, T cell proliferation and IFN- γ production have been correlated with peptide-MHC affinity (26). Together, the multi-scale model incorporates the molecular-, cellular-, tissue-, and organ/organism-scale models and allows us to explore, among other things, the relevance of peptide-MHC affinity differences to the overall immune response.

Scale	Model Description	Model Inputs	Model Outputs
Molecular	Peptide-MHC binding model	Training data (peptide sequence, binding affinities)	Peptide-MHC II affinity
Cellular	Single-APC model	Antigen and IFN- γ concentrations; cellular parameters	Surface pMHC complexes
Tissue	Cellular interactions in a single LN	Antigen concentration cell numbers; cellular and LN parameters	Number of effector cells exiting the LN
Organ/organism	Two-compartment models of LN + other sites of interest	Antigen; cell numbers; cell, LN and tissue parameters	Pathogen numbers (i.e. viral or bacterial load)

Table 2. Description of each of the four individual-scale models.
APC=antigen presenting cell , LN=lymph nodes.

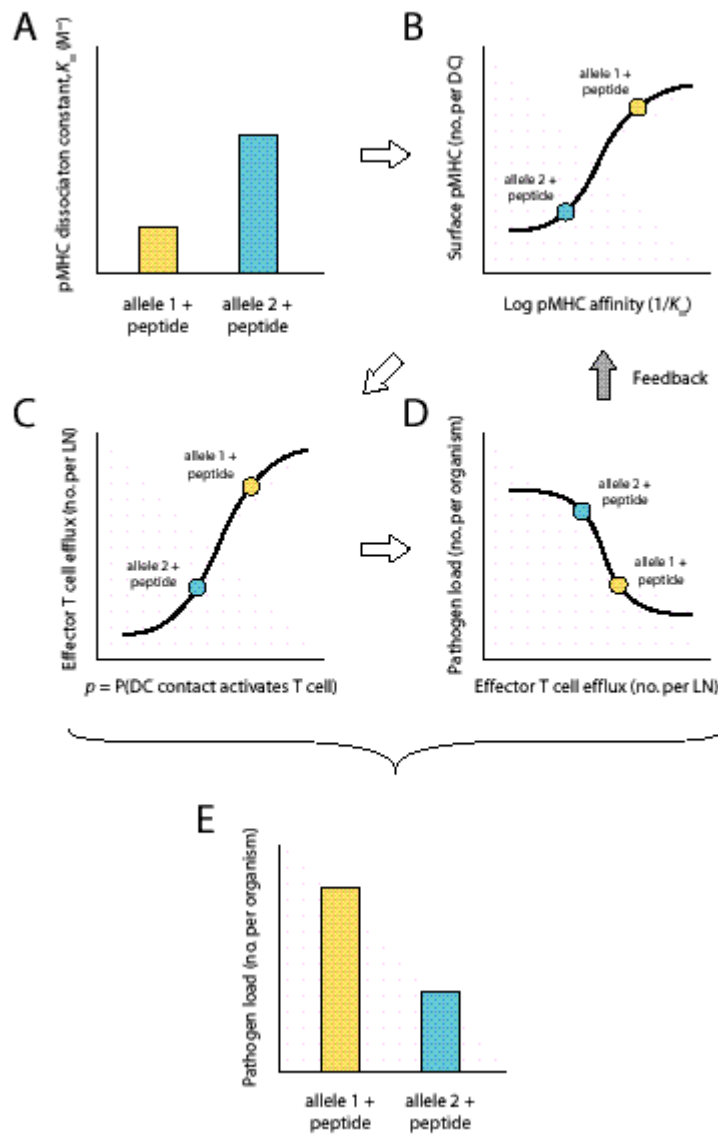


Figure 10

In a similar fashion, the impact of combinations of parameters might be explored. For example, can a higher peptide-MHC affinity compensate for poorer APC uptake ability? As shown in *Fig. 11A*, there is indeed such a relationship between affinity and uptake rate. Can a higher peptide-MHC affinity compensate for fewer APCs or fewer highly

specific T cells? As shown in *Fig. 11B*, there is a tradeoff between affinity and the number of mature DCs required to enter the LN in order to produce a particular number of effector T cells. In this figure, affinity is represented as part of the aggregate parameter p , the probability that a $CD4^+$ T cell becomes activated after contact with a DC; p increases with the number of pMHC displayed, which in turn increases with pMHC affinity (see *Fig. 5D*). This suggests that an increase in the number of cells presenting antigen within the LN can compensate for a reduced affinity between peptide and MHC or lower numbers of pMHC on the surface of the DC (both factors captured by the probability p). A similar result holds for the number of T cells present that can recognize the antigen being presented (data not shown). Thus, although at present we are still in the early stages of integrating our individual-scale models, we can already begin to address some of the multi-scale questions posed earlier, in particular those that do not require integration of all four scales.

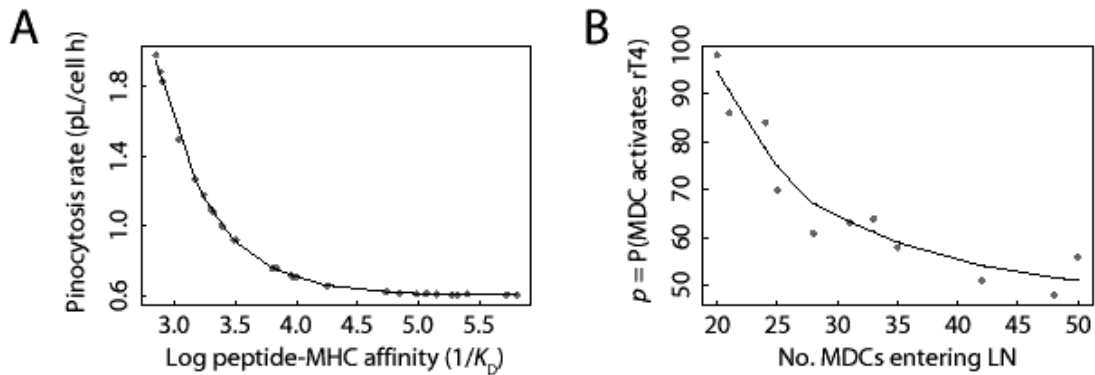


Figure 11

We described above a hierarchical approach to our multi-scale model of antigen presentation. However, at a later stage in model development we may need to incorporate feedback from larger scales to smaller scales, moving us to a hybrid approach. Information on the local environment in the LN, for example cytokine concentrations, could be passed back to the APC model to allow cytokine concentrations to influence the number of pMHCs on the APC surface. Furthermore, many intracellular pathogens, including *Mtb*, inhibit antigen presentation within macrophages. While the mediators of this effect, including 19-kDa lipoprotein (163, 164, 165, 166), act on molecular-scale events within macrophages, the total production of such mediators is likely to depend on the number of pathogens at the site of infection, a tissue-scale quantity. However, the latter quantity can only be predicted after accounting for other tissue-scale factors such as the activation state of macrophages and T helper cells at the site of infection. In this example, then, tissue-scale events feed back on molecular-scale events and vice versa.

Most importantly, once a multi-scale model is developed, it can be applied toward the generation of hypotheses regarding the role of antigen presentation in immunity. For example, recall that there is a clear association between particular MHC alleles and disease susceptibility/resistance. If our molecular-scale model shows that there is a link between particular MHC alleles and affinities for particular antigens, then the full multi-

scale model could be used to show the expected outcome at the system scale (Chang *et al.*, submitted).

As another example, the efficacy of a vaccine is in part determined by activation of CD4⁺ T cells. A multi-scale model will enable testing of the roles that various factors play in that activation. What is the relationship between antigen dose in the vaccine and the number of mature DCs appearing in a LN? What level of T cell activation is necessary to generate an appropriate memory response (one further possible extension of the multi-scale model) that is critical for vaccines to be effective against later challenge? Further, what aspects of the antigen presentation process should be targeted to optimize vaccine efficacy? Can such insights help explain why BCG, the vaccine against TB used for the last 80 years, has failed to eliminate TB? Finding the answers to such questions may rely at least in part on the developments described in this review.

Looking Ahead

The ultimate goal of developing mathematical/computational models of biological systems is to use these models to better understand the systems and to suggest mechanisms to manipulate the systems, i.e. to treat or prevent disease. For example, one can introduce therapeutic modulation, even modes unapproachable using current medical techniques, in a controlled manner in order to evaluate potential targets for both treatment and vaccine strategies. Indeed, the FDA Critical Path Initiative (167) has recently identified model-based drug development, including drug and disease modeling, as an important goal.

There are numerous challenges ahead for the development of multi-scale models in biology and for antigen presentation in particular. First, there is a need for experimental data to allow for model validation at every scale. For example, although model development is an essential part to predicting peptide-MHC affinities, the quality and amount of data available to develop models remains an issue (168, 169, 120). The predictive ability of a model should improve with the size of the training set. Currently databases contain 13000-24000 peptides, though the sizes of these databases can be misleading. Labs often generate very closely related peptides to determine characteristics of binding; these peptides are then listed as separate entries in the databases. However, using homologous peptides to fit models of peptide-MHC binding can skew predictions. Methods to eliminate homologous peptides are available (170, 171) and, when implemented, significantly reduce data set size.

From a computational perspective, methods for integrating predictions at individual scales and for allowing behavior at each scale to influence behavior at other scales are needed and are currently under development for a number of biological systems (172). In addition, a number of groups are developing platforms with the explicit aim of standardizing models; this would make it easier to pass models from one research group to another (173-175).

In sum, nearly all biological processes involve multiple scales. Thus the lessons learned here regarding the use of modeling to integrate molecular-, cellular-, tissue-, and organ/organism-scale events can inform studies on a broad range of biological systems and provide tools to analyze them.

Figure legends

Fig. 1. Key events in antigen presentation. Biological scales are represented here as physical scales. (A) Multi-compartmental system of blood, lymphatics, and particular organs/sites of interest. (B) Lymph node environment wherein antigen-presenting cells (APCs) interact with T cells. (C) Intracellular pathways leading to peptide-MHC class II (pMHC) complexes on the surface of an APC. (D) Molecular-level interactions between peptide and MHC are influenced by genetic differences among MHC II alleles.

Fig. 2. Molecular and intracellular events influencing the display of peptide-MHC II complexes on a single antigen-presenting cell. One-step reactions are indicated by solid arrows while regulatory processes (which may involve several reactions) are indicated by dashed arrows.

Fig. 3. Antigen-presenting cells (APCs) and T cells interacting in the lymph node (LN). (A) Schematic of the LN. Afferent lymphatics empty into a LN, bringing APCs such as DCs that rarely leave the LN after arrival. T cells enter from the blood through the HEVs and exit via the efferent lymph. Dynamic interactions between APCs and T cells occur within the LN. (B) Intravital microscopy image showing the interaction of DCs (green) with T cells (red) within a section of the lymph node measuring 75 μm by 100 μm . Image from (60), courtesy of *J. Exp. Med.* and Mark Miller. (C) Lattice representation of a LN. A 7x7 grid is shown, where each unit space is the size of one DC, the largest cell type of those included in our simulations. T4 = CD4^+ T cell; T8 = CD8^+ T cell; DC = dendritic cell; r = resting; a = activated; e = effector; M=mature; L = licensed.

Fig. 4. Algorithms to predict peptide-MHC binding. (A) On the left we show three steps common to most algorithms: training data selection, algorithm fitting or training, and testing. On the right we show two modifications that we have proposed making to these algorithms to improve prediction of longer peptides (i.e. those greater than nine amino acids in length). These modifications are intended to account for PFR-MHC interactions and register shifting. (B) Performance of one published algorithm, ISC-PLS (107), before and after modifications proposed in Panel A, on training and test sets for two MHC II alleles.

Fig. 5. Model of a single antigen-presenting cell (APC). Ordinary differential equations were written based on the events shown in Figure 2. (A) Model simulation of CIITA mRNA and MHC II mRNA levels in macrophages following $\text{IFN-}\gamma$ treatment

representing a positive control. (B) Experimental data (176) for comparison with panel A. (C) Comparison of the antigen-presenting abilities of macrophages and DCs. Macrophage parameter values (i.e. baseline) were taken from (131). Two parameters were changed to simulate DCs: rate constants for uptake and MHC II expression (132, 133). (D) Number of surface pMHC complexes as a function of pMHC affinity ($1/K_D$) in macrophages three hours following addition of antigen. (E) Partial rank correlation coefficients for three parameters (k_{txn} , k_{out} , k_{pino}) at three time points (1, 10 and 100 hours following addition of antigen). k_{txn} = MHC II transcription rate constant; k_{out} = rate constant for trafficking of pMHC to the cell surface; k_{pino} = pinocytosis rate constant.

Fig. 6. Rule for T cell activation within the agent-based model (ABM). If a mature dendritic cell (MDC) and a resting (and naïve) CD4^+ T cell (rT4) are in neighboring microcompartments, then there is a probability p that the resting cell will become activated.

Fig. 7. Cell dynamics in the simulated LN. (A) Snapshot of cells in the LN at ≈ 42 hours after introduction of 6 MDCs onto the ABM lattice at day 0 of the simulation. Initial conditions were 250 resting CD4^+ T cells, 125 resting CD8^+ T cells, and 5 immature DCs. A complete list of rules can be seen in (Bajaria *et al.*, submitted). (B) Temporal dynamics of all cell populations in the simulation. Cell types are as defined in Fig. 3.

Fig. 8. Effect of variation in the probability of activating resting CD4^+ T cells in the ABM model. The parameter p represents the probability of activation of a resting CD4^+ T cell upon interaction with a cognate MDC and is varied from 0.05 to 0.95. (A) The number of activated CD4^+ T cells produced at a given time point increases with p . (B) Likewise, the number of activated CD8^+ T cells produced at a given time point also increases with p . In this figure, 16 MDCs were introduced on day 0.

Fig. 9. Two-compartment models of LN linked to another system. (A) LN-blood model. CD4^+ T cells, CD8^+ T cells, and DCs traffic between these two compartments. (B) LN-lung model. DCs, macrophages ($\text{M}\Phi$) and CD4^+ T cells traffic between these two compartments. Cell types are as defined in Fig. 3.

Fig. 10. Building a multi-scale model of antigen presentation from four individual scale models. In the particular example shown, the relevance of allele-specific differences in peptide-MHC II affinity to antigen presentation and the overall immune response are explored. Predictions from each scale are fed to the next larger-scale model, providing predictions between adjacent (A-D) and non-adjacent (E) scales; i.e. a hierarchical approach is used. A hybrid approach must be used if feedback from larger scales to smaller scales is present, for example if overall pathogen load can affect intracellular events.

Fig. 11. Tradeoffs between processes in the models. (A) The relationship between uptake rate and peptide-MHC II affinity in producing pMHC complexes in the APC model (Fig. 2). Each point represents a pair of compensatory parameter values that

results in ≈ 200 pMHC complexes on the APC surface three hours after antigen is added to macrophages. (Other parameters were as published in 131). (B) The relationship between the probability of activation of resting (naïve) $CD4^+$ T cells versus the number of mature DCs that enter the LN on day 0 in generating activated $CD4^+$ T cells in the ABM. Each point represents a pair of compensatory parameter values that results in 330 ± 30 effector $CD4^+$ T cells generated. This result represents the 42-hour time point. In both (A) and (B) a local regression line has been fitted to the data.

Acknowledgements

This work was supported under grant numbers HL68526, HL72682, and LM00902701. The authors thank Simeone Marino and Seema Bajaria for use of results from their published work.

1. Savageau MA. Reconstructionist molecular biology. *New Biol* 1991;**3**(2):190-7.
2. Hunter P, Nielsen P. A strategy for integrative computational physiology. *Physiology* (Bethesda) 2005;**20**:316-25.
3. Bassingthwaite JB, Chizeck HJ, Atlas LE, Qian H. Multiscale modeling of cardiac cellular energetics. *Ann N Y Acad Sci* 2005;**1047**:395-424.
4. Choe Y. The role of temporal parameters in a thalamocortical model of analogy. *IEEE Trans Neural Netw* 2004;**15**(5):1071-82.
5. Breakspear M, Stam CJ. Dynamics of a neural system with a multiscale architecture. *Philos Trans R Soc Lond B Biol Sci* 2005;**360**(1457):1051-74.
6. Robinson PA, Rennie CJ, Rowe DL, O'Connor SC, Gordon E. Multiscale brain modelling. *Philos Trans R Soc Lond B Biol Sci* 2005;**360**(1457):1043-50.
7. Alarcon T, Byrne HM, Maini PK. Towards whole-organ modelling of tumour growth. *Prog Biophys Mol Biol* 2004;**85**(2-3):451-72.
8. Peirce SM, Skalak TC. Microvascular remodeling: a complex continuum spanning angiogenesis to arteriogenesis. *Microcirculation* 2003;**10**(1):99-111.
9. Reeves GT, Kalifa R, Klein DE, Lemmon MA, Shvartsman SY. Computational analysis of EGFR inhibition by Argos. *Dev Biol* 2005;**284**(2):523-35.
10. Glotzer SC, Paul W. Molecular and mesoscale simulation methods for polymer materials. *Annual Review of Materials Research* 2002;**32**:401-436.
11. Comisar WA, Hsiong SX, Kong HJ, Mooney DJ, Linderman JJ. Multi-scale modeling to predict ligand presentation within RGD nanopatterned hydrogels. *Biomaterials* 2006;**27**(10):2322-2329.
12. De Libero G, Mori L. Recognition of lipid antigens by T cells. *Nat Rev Immunol* 2005;**5**(6):485-96.
13. Cheng Y, Prusoff WH. Relationship between the inhibition constant (K_i) and the concentration of inhibitor which causes 50 per cent inhibition (I_{50}) of an enzymatic reaction. *Biochem Pharmacol* 1973;**22**(23):3099-108.
14. Sette A, Buus S, Colon S, Miles C, Grey HM. Structural analysis of peptides capable of binding to more than one Ia antigen. *J Immunol* 1989;**142**(1):35-40.

15. Roche PA, Cresswell P. High-affinity binding of an influenza hemagglutinin-derived peptide to purified HLA-DR. *J Immunol* 1990;**144**(5):1849-56.
16. Southwood S, Sidney J, Kondo A, del Guercio MF, Appella E, Hoffman S, *et al.* Several common HLA-DR types share largely overlapping peptide binding repertoires. *J Immunol* 1998;**160**(7):3363-73.
17. Dedier S, Reinelt S, Rion S, Folkers G, Rognan D. Use of fluorescence polarization to monitor MHC-peptide interactions in solution. *J Immunol Methods* 2001;**255**(1-2):57-66.
18. Brusic V, Rudy G, Honeyman G, Hammer J, Harrison L. Prediction of MHC class II-binding peptides using an evolutionary algorithm and artificial neural network. *Bioinformatics* 1998; **14**: 121-130.
19. Bhasin M, Singh H, Raghava GP. MHCBN: a comprehensive database of MHC binding and non-binding peptides. *Bioinformatics* 2003;**19**(5):665-6.
20. Toseland CP, Clayton DJ, McSparron H, Hemsley SL, Blythe MJ, Paine K, *et al.* AntiJen: a quantitative immunology database integrating functional, thermodynamic, kinetic, biophysical, and cellular data. *Immunome Res* 2005;**1**(1):4.
21. Sette A, Vitiello A, Rehman B, Fowler P, Nayarsina R, Kast WM, *et al.* The relationship between class I binding affinity and immunogenicity of potential cytotoxic T cell epitopes. *J Immunol* 1994;**153**(12):5586-92.
22. Vukmanovic S, Neubert TA, Santori FR. Could TCR antagonism explain associations between MHC genes and disease? *Trends Mol Med* 2003;**9**(4):139-46.
23. Rajagopalan S, Long EO. Understanding how combinations of HLA and KIR genes influence disease. *J Exp Med* 2005;**201**(7):1025-9.
24. Thorsby E, Lie BA. HLA associated genetic predisposition to autoimmune diseases: Genes involved and possible mechanisms. *Transpl Immunol* 2005;**14**(3-4):175-82.
25. Geluk A, Taneja V, van Meijgaarden KE, Zanelli E, Abou-Zeid C, Thole JE, *et al.* Identification of HLA class II-restricted determinants of Mycobacterium tuberculosis-derived proteins by using HLA-transgenic, class II-deficient mice. *Proc Natl Acad Sci U S A* 1998;**95**(18):10797-802.
26. Hill JA, Wang D, Jevnikar AM, Cairns E, Bell DA. The relationship between predicted peptide-MHC class II affinity and T-cell activation in a HLA-DRbeta1*0401 transgenic mouse model. *Arthritis Res Ther* 2003;**5**(1):R40-8.
27. Bryant P, Ploegh H. Class II MHC peptide loading by the professionals. *Curr Opin Immunol* 2004;**16**(1):96-102.
28. Honey K, Rudensky AY. Lysosomal cysteine proteases regulate antigen presentation. *Nat Rev Immunol* 2003;**3**(6):472-82.
29. Denzin LK, Cresswell P. HLA-DM induces CLIP dissociation from MHC class II alpha beta dimers and facilitates peptide loading. *Cell* 1995;**82**(1):155-65.
30. Adorini L, Muller S, Cardinaux F, Lehmann PV, Falcioni F, Nagy ZA. In vivo competition between self peptides and foreign antigens in T-cell activation. *Nature* 1988;**334**(6183):623-5.
31. Chicz RM, Urban RG, Gorga JC, Vignali DA, Lane WS, Strominger JL. Specificity and promiscuity among naturally processed peptides bound to HLA-DR alleles. *J Exp Med* 1993;**178**(1):27-47.

32. Chomarat P, Banchereau J, Davoust J, Palucka AK. IL-6 switches the differentiation of monocytes from dendritic cells to macrophages. *Nat Immunol* 2000;**1**(6):510-4.
33. Chomarat P, Dantin C, Bennett L, Banchereau J, Palucka AK. TNF skews monocyte differentiation from macrophages to dendritic cells. *J Immunol* 2003;**171**(5):2262-9.
34. Fogg DK, Sibon C, Miled C, Jung S, Aucouturier P, Littman DR, *et al.* A clonogenic bone marrow progenitor specific for macrophages and dendritic cells. *Science* 2006;**311**(5757):83-7.
35. Inaba K, Steinman RM. Protein-specific helper T-lymphocyte formation initiated by dendritic cells. *Science* 1985;**229**(4712):475-9.
36. Inaba K, Pack M, Inaba M, Sakuta H, Isdell F, Steinman RM. High levels of a major histocompatibility complex II-self peptide complex on dendritic cells from the T cell areas of lymph nodes. *J Exp Med* 1997;**186**(5):665-72.
37. Reinhardt RL, Khoruts A, Merica R, Zell T, Jenkins MK. Visualizing the generation of memory CD4 T cells in the whole body. *Nature* 2001;**410**(6824):101-5.
38. Kimachi K, Croft M, Grey HM. The minimal number of antigen-major histocompatibility complex class II complexes required for activation of naive and primed T cells. *Eur J Immunol* 1997;**27**(12):3310-7.
39. Irvine DJ, Purbhoo MA, Krogsgaard M, Davis MM. Direct observation of ligand recognition by T cells. *Nature* 2002;**419**(6909):845-9.
40. Watts TH. T cell activation by preformed, long-lived Ia-peptide complexes. Quantitative aspects. *J Immunol* 1988;**141**(11):3708-14.
41. Agrawal NG, Linderman JJ. Mathematical modeling of helper T lymphocyte/antigen-presenting cell interactions: analysis of methods for modifying antigen processing and presentation. *J Theor Biol* 1996;**182**(4):487-504.
42. Lavoie PM, Dumont AR, McGrath H, Kernaleguen AE, Sekaly RP. Delayed expansion of a restricted T cell repertoire by low-density TCR ligands. *Int Immunol* 2005;**17**(7):931-41.
43. von Andrian UH, Mempel TR. Homing and cellular traffic in lymph nodes. *Nat Rev Immunol* 2003;**3**(11):867-78.
44. Marchesi VT, Gowans JL. The Migration of Lymphocytes through the Endothelium of Venules in Lymph Nodes: An Electron Microscope Study. *Proc R Soc Lond B Biol Sci* 1964;**159**:283-90.
45. Girard JP, Springer TA. High endothelial venules (HEVs): specialized endothelium for lymphocyte migration. *Immunol Today* 1995;**16**(9):449-57.
46. Davis DM, Dustin ML. What is the importance of the immunological synapse? *Trends Immunol* 2004;**25**(6):323-7.
47. Lee KH, Dinner AR, Tu C, Campi G, Raychaudhuri S, Varma R, *et al.* The immunological synapse balances T cell receptor signaling and degradation. *Science* 2003;**302**(5648):1218-22.
48. Butcher EC, Picker LJ. Lymphocyte homing and homeostasis. *Science* 1996;**272**(5258):60-6.
49. von Andrian UH, Mackay CR. T-cell function and migration. Two sides of the same coin. *N Engl J Med* 2000;**343**(14):1020-34.

50. Chain B, McCafferty I, Wallace G, Askenase PW. Improvement of the in vitro T cell proliferation assay by a modified method that separates the antigen recognition and IL-2-dependent steps. *J Immunol Methods* 1987;**99**(2):221-8.
51. Traynor TR, Herring AC, Dorf ME, Kuziel WA, Toews GB, Huffnagle GB. Differential roles of CC chemokine ligand 2/monocyte chemotactic protein-1 and CCR2 in the development of T1 immunity. *J Immunol* 2002;**168**(9):4659-66.
52. Algood HM, Flynn JL. CCR5-deficient mice control Mycobacterium tuberculosis infection despite increased pulmonary lymphocytic infiltration. *J Immunol* 2004;**173**(5):3287-96.
53. Lazarevic V, Nolt D, Flynn JL. Long-term control of Mycobacterium tuberculosis infection is mediated by dynamic immune responses. *J Immunol* 2005;**175**(2):1107-17.
54. Lindell DM, Moore TA, McDonald RA, Toews GB, Huffnagle GB. Distinct compartmentalization of CD4+ T-cell effector function versus proliferative capacity during pulmonary cryptococcosis. *Am J Pathol* 2006;**168**(3):847-55.
55. Sumen C, Mempel TR, Mazo IB, von Andrian UH. Intravital microscopy: visualizing immunity in context. *Immunity* 2004;**21**(3):315-329.
56. Catron DM, Itano AA, Pape KA, Mueller DL, Jenkins MK. Visualizing the first 50 hr of the primary immune response to a soluble antigen. *Immunity* 2004;**21**(3):341-7.
57. Miller MJ, Wei SH, Cahalan MD, Parker I. Autonomous T cell trafficking examined in vivo with intravital two-photon microscopy. *Proc Natl Acad Sci U S A* 2003;**100**(5):2604-9.
58. Meyer-Hermann ME, Maini PK. Interpreting two-photon imaging data of lymphocyte motility. *Phys Rev E Stat Nonlin Soft Matter Phys* 2005;**71**(6 Pt 1):061912.
59. Sprent J, Tough D. T cell death and memory. *Science* 2001; **293**: 245-248.
60. Miller MJ, Safrina O, Parker I, Cahalan MD. Imaging the single cell dynamics of CD4+ T cell activation by dendritic cells in lymph nodes. *J Exp Med* 2004;**200**(7):847-56.
61. Miyasaka M, Tanaka T. Lymphocyte trafficking across high endothelial venules: dogmas and enigmas. *Nat Rev Immunol* 2004;**4**(5):360-70.
62. Cahill RN, Frost H, Trnka Z. The effects of antigen on the migration of recirculating lymphocytes through single lymph nodes. *J Exp Med* 1976;**143**(4):870-88.
63. Gretz JE, Anderson AO, Shaw S. Cords, channels, corridors and conduits: critical architectural elements facilitating cell interactions in the lymph node cortex. *Immunol Rev* 1997;**156**:11-24.
64. Bajenoff M, Granjeaud S, Guerder S. The strategy of T cell antigen-presenting cell encounter in antigen-draining lymph nodes revealed by imaging of initial T cell activation. *J Exp Med* 2003;**198**(5):715-24.
65. Randolph GJ, Angeli V, Swartz MA. Dendritic-cell trafficking to lymph nodes through lymphatic vessels. *Nat Rev Immunol* 2005;**5**(8):617-28.
66. Westermann J, Bode U, Pabst R. Migration of naive and memory T cells in vivo. *Immunol Today* 1998;**19**(3):143-4.
67. Rosenberg YJ, Janosy G. The importance of lymphocyte trafficking in regulating blood lymphocyte levels during HIV and SIV infections. *Semin Immunol* 1999;**11**(2):139-54.

68. Miller MJ, Hejazi AS, Wei SH, Cahalan MD, Parker I. T cell repertoire scanning is promoted by dynamic dendritic cell behavior and random T cell motility in the lymph node. *Proc Natl Acad Sci U S A* 2004;**101**(4):998-1003.
69. Marino S, Kirschner DE. The human immune response to *Mycobacterium tuberculosis* in lung and lymph node. *J Theor Biol* 2004;**227**(4):463-86.
70. Marino S, Pawar S, Fuller CL, Reinhart TA, Flynn JL, Kirschner DE. Dendritic cell trafficking and antigen presentation in the human immune response to *Mycobacterium tuberculosis*. *J Immunol* 2004;**173**(1):494-506.
71. Sprent J. Circulating T and B lymphocytes of the mouse. I. Migratory properties. *Cell Immunol* 1973;**7**(1):10-39.
72. Sprent J, Basten A. Circulating T and B lymphocytes of the mouse. II. Lifespan. *Cell Immunol* 1973;**7**(1):40-59.
73. Swain SL, Croft M, Dubey C, Haynes L, Rogers P, Zhang X, *et al.* From naive to memory T cells. *Immunol Rev* 1996;**150**:143-67.
74. Mims CA, Nash A, Stephen J. Mims' Pathogenesis of infectious disease. 5th ed. San Diego: Academic Press, 2001.
75. Miller DM, Rahill BM, Boss JM, Lairmore MD, Durbin JE, Waldman JW, *et al.* Human cytomegalovirus inhibits major histocompatibility complex class II expression by disruption of the Jak/Stat pathway. *J Exp Med* 1998;**187**(5):675-83.
76. Mahanty S, Hutchinson K, Agarwal S, McRae M, Rollin PE, Pulendran B. Cutting edge: impairment of dendritic cells and adaptive immunity by Ebola and Lassa viruses. *J Immunol* 2003;**170**(6):2797-801.
77. Fenton MJ. Macrophages and tuberculosis. *Curr Opin Hematol* 1998;**5**(1):72-8.
78. Moreno C, Mehlert A, Lamb J. The inhibitory effects of mycobacterial lipoarabinomannan and polysaccharides upon polyclonal and monoclonal human T cell proliferation. *Clin Exp Immunol* 1988;**74**(2):206-10.
79. Hmama Z, Gabathuler R, Jefferies WA, de Jong G, Reiner NE. Attenuation of HLA-DR expression by mononuclear phagocytes infected with *Mycobacterium tuberculosis* is related to intracellular sequestration of immature class II heterodimers. *J Immunol* 1998;**161**(9):4882-93.
80. Noss EH, Harding CV, Boom WH. *Mycobacterium tuberculosis* inhibits MHC class II antigen processing in murine bone marrow macrophages. *Cell Immunol* 2000;**201**(1):63-74.
81. [unaids.org](http://www.unaids.org). UNAIDS/WHO AIDS epidemic update: December 2005. <http://www.unaids.org>, 2005.
82. Edelstein-Keshet L. *Mathematical Models In Biology*: McGraw-Hill Companies, 1988.
83. Murray JD. *Mathematical biology*. Berlin ; New York: Springer-Verlag, 1989.
84. Keener JP, Sneyd J. *Mathematical physiology*. New York: Springer, 1998.
85. Segel LA, Cohen IR. *Design principles for the immune system and other distributed autonomous systems*. Oxford ; New York: Oxford University Press, 2001.
86. Grimm V, Railsback SF. *Individual-based modeling and ecology*. Princeton: Princeton University Press, 2005.
87. Lauffenburger DA, Linderman JL. *Receptors: models for binding, trafficking and signaling*. New York, NY: Oxford University Press, 1993.

88. Brauer F, Castillo-Châavez C. Mathematical models in population biology and epidemiology. New York: Springer, 2001.
89. Armitage P, Berry G, Matthews JNS. Statistical methods in medical research. 4th ed. Malden, MA: Blackwell Science, 2001.
90. Lund O. Immunological bioinformatics. Cambridge, Ma: MIT Press, 2005.
91. Ewens WJ, Grant GR. Statis[t]ical methods in bioinformatics : an introduction. 2nd ed. New York, N.Y.: Springer, 2005.
92. DeAngelis DL, Gross LJ. Individual-based models and approaches in ecology : populations, communities, and ecosystems. New York: Chapman & Hall, 1992.
93. Kirschner DE, Gammack D, Ganguli S, Marino S, Segovia-Juarez J. Understanding the Immune Response in Tuberculosis Using Different Mathematical Models and Biological Scales. Society for Industrial and Applied Mathematics 2005;**3**(2):312-345.
94. Waller A, Sutton KL, Kinzer-Ursem TL, Absood A, Traynor JR, Linderman JJ, *et al.* Receptor binding kinetics and cellular responses of six N-formyl peptide agonists in human neutrophils. Biochemistry 2004;**43**(25):8204-16.
95. Blower SM, Dowlatabadi H. Sensitivity and Uncertainty Analysis of Complex-Models of Disease Transmission - An HIV Model, as an Example. International Statistical Review 1994;**62**(2):229-243.
96. Helton JC, Davis FJ. Illustration of sampling-based methods for uncertainty and sensitivity analysis. Risk Anal 2002;**22**(3):591-622.
97. Gammack D, Doering CR, Kirschner DE. Macrophage response to Mycobacterium tuberculosis infection. J Math Biol 2004;**48**(2):218-42.
98. Segovia-Juarez JL, Ganguli S, Kirschner D. Identifying control mechanisms of granuloma formation during M. tuberculosis infection using an agent-based model. J Theor Biol 2004;**231**(3):357-76.
99. Meng X-l, Rosenthal R, Rubin DB. Comparing correlated correlation coefficients. Psychological Bulletin 1992;**111**(1):172-175.
100. Rammensee HG. Chemistry of peptides associated with MHC class I and class II molecules. Curr Opin Immunol 1995;**7**(1):85-96.
101. Parker KC, Bednarek MA, Coligan JE. Scheme for ranking potential HLA-A2 binding peptides based on independent binding of individual peptide side-chains. J Immunol 1994;**152**(1):163-75.
102. Murugan N, Dai Y. Prediction of MHC class II binding peptides based on an iterative learning model. Immunome Res 2005;**1**:6.
103. Mallios RR. Class II MHC quantitative binding motifs derived from a large molecular database with a versatile iterative stepwise discriminant analysis meta-algorithm. Bioinformatics 1999;**15**(6):432-9.
104. Mallios RR. Predicting class II MHC/peptide multi-level binding with an iterative stepwise discriminant analysis meta-algorithm. Bioinformatics 2001;**17**(10):942-8.
105. Mallios RR. A consensus strategy for combining HLA-DR binding algorithms. Hum Immunol 2003;**64**(9):852-6.
106. Doytchinova IA, Flower DR. Quantitative approaches to computational vaccinology. Immunol Cell Biol 2002;**80**(3):270-9.

107. Doytchinova IA, Flower DR. Towards the in silico identification of class II restricted T-cell epitopes: a partial least squares iterative self-consistent algorithm for affinity prediction. *Bioinformatics* 2003;**19**(17):2263-70.
108. Honeyman MC, Brusica V, Stone NL, Harrison LC. Neural network-based prediction of candidate T-cell epitopes. *Nat Biotechnol* 1998;**16**(10):966-9.
109. Milik M, Sauer D, Brunmark AP, Yuan L, Vitiello A, Jackson MR, *et al.* Application of an artificial neural network to predict specific class I MHC binding peptide sequences. *Nat Biotechnol* 1998;**16**(8):753-6.
110. Buus S, Lauemoller SL, Wornig P, Kesmir C, Frimurer T, Corbet S, *et al.* Sensitive quantitative predictions of peptide-MHC binding by a 'Query by Committee' artificial neural network approach. *Tissue Antigens* 2003;**62**(5):378-84.
111. Noguchi H, Kato R, Hanai T, Matsubara Y, Honda H, Brusica V, *et al.* Hidden Markov model-based prediction of antigenic peptides that interact with MHC class II molecules. *J Biosci Bioeng* 2002;**94**(3):264-70.
112. Zhao Y, Pinilla C, Valmori D, Martin R, Simon R. Application of support vector machines for T-cell epitopes prediction. *Bioinformatics* 2003;**19**(15):1978-84.
113. Bhasin M, Raghava GP. Prediction of CTL epitopes using QM, SVM and ANN techniques. *Vaccine* 2004;**22**(23-24):3195-204.
114. Altuvia Y, Sette A, Sidney J, Southwood S, Margalit H. A structure-based algorithm to predict potential binding peptides to MHC molecules with hydrophobic binding pockets. *Hum Immunol* 1997;**58**(1):1-11.
115. Schueler-Furman O, Altuvia Y, Sette A, Margalit H. Structure-based prediction of binding peptides to MHC class I molecules: application to a broad range of MHC alleles. *Protein Sci* 2000;**9**(9):1838-46.
116. Altuvia Y, Margalit H. A structure-based approach for prediction of MHC-binding peptides. *Methods* 2004;**34**(4):454-9.
117. Bui HH, Schiewe AJ, von Grafenstein H, Haworth IS. Structural prediction of peptides binding to MHC class I molecules. *Proteins* 2006;**63**(1):43-52.
118. Fagerberg T, Cerottini JC, Michielin O. Structural prediction of peptides bound to MHC class I. *J Mol Biol* 2006;**356**(2):521-46.
119. Yu K, Petrovsky N, Schonbach C, Koh JY, Brusica V. Methods for prediction of peptide binding to MHC molecules: a comparative study. *Mol Med* 2002;**8**(3):137-48.
120. Brusica V, Bajic VB, Petrovsky N. Computational methods for prediction of T-cell epitopes--a framework for modelling, testing, and applications. *Methods* 2004;**34**(4):436-43.
121. Rammensee H, Bachmann J, Emmerich NP, Bachor OA, Stevanovic S. SYFPEITHI: database for MHC ligands and peptide motifs. *Immunogenetics* 1999;**50**(3-4):213-9.
122. Raghava GP. MHC Bench - Evaluation of MHC Binding Peptide Prediction Algorithms - <http://www.imtech.res.in/raghava/mhcbench>.
123. Sercarz EE, Maverakis E. Mhc-guided processing: binding of large antigen fragments. *Nat Rev Immunol* 2003;**3**(8):621-9.
124. Nielsen M, Lundegaard C, Wornig P, Hvid CS, Lamberth K, Buus S, *et al.* Improved prediction of MHC class I and class II epitopes using a novel Gibbs sampling approach. *Bioinformatics* 2004;**20**(9):1388-97.

125. Bartnes K, Leon F, Briand JP, Travers PJ, Hannestad K. N-terminal elongation of a peptide determinant beyond the first primary anchor improves binding to H-2 I-Ad and HLA-DR1 by backbone-dependent and aromatic side chain-dependent interactions, respectively. *Eur J Immunol* 1999;**29**(1):189-95.
126. Fleckenstein B, Jung G, Wiesmuller KH. Quantitative analysis of peptide-MHC class II interaction. *Semin Immunol* 1999;**11**(6):405-16.
127. Petrovsky N, Brusica V. Virtual models of the HLA class I antigen processing pathway. *Methods* 2004;**34**(4):429-35.
128. Donnes P, Kohlbacher O. Integrated modeling of the major events in the MHC class I antigen processing pathway. *Protein Sci* 2005;**14**(8):2132-40.
129. Singer DF, Linderman JJ. The relationship between antigen concentration, antigen internalization, and antigenic complexes: modeling insights into antigen processing and presentation. *J Cell Biol* 1990;**111**(1):55-68.
130. Singer DF, Linderman JJ. Antigen processing and presentation: how can a foreign antigen be recognized in a sea of self proteins? *J Theor Biol* 1991;**151**(3):385-404.
131. Chang ST, Linderman JJ, Kirschner DE. Multiple mechanisms allow *Mycobacterium tuberculosis* to continuously inhibit MHC class II-mediated antigen presentation by macrophages. *Proc Natl Acad Sci U S A* 2005;**102**(12):4530-5.
132. Sallusto F, Cella M, Danieli C, Lanzavecchia A. Dendritic cells use macropinocytosis and the mannose receptor to concentrate macromolecules in the major histocompatibility complex class II compartment: downregulation by cytokines and bacterial products. *J Exp Med* 1995;**182**(2):389-400.
133. Laupeze B, Fardel O, Onno M, Bertho N, Drenou B, Fauchet R, *et al.* Differential expression of major histocompatibility complex class Ia, Ib, and II molecules on monocytes-derived dendritic and macrophagic cells. *Hum Immunol* 1999;**60**(7):591-7.
134. Segel LA. Modeling dynamic phenomena in molecular and cellular biology. Cambridge ; New York: Cambridge University Press, 1984.
135. Gammack D, Ganguli S, Marino S, Segovia-Juarez JL, Kirschner D. Understanding granuloma formation using different mathematical and biological scales. *SIAM Journal of Multiscale Modeling and Simulation* 2005;**3**:312-345.
136. Stoll S, Delon J, Brotz TM, Germain RN. Dynamic imaging of T cell-dendritic cell interactions in lymph nodes. *Science* 2002;**296**(5574):1873-6.
137. Jacquez JA. Compartmental Analysis in Biology and Medicine. 3rd ed. Ann Arbor, MI: BioMedware, 1996.
138. Bajaria SH, Webb G, Cloyd M, Kirschner D. Dynamics of naive and memory CD4+ T lymphocytes in HIV-1 disease progression. *J Acquir Immune Defic Syndr* 2002;**30**(1):41-58.
139. Ye P, Kourtis A, Kirschner D. The effects of different HIV type 1 strains of human thymic function. *AIDS Res Hum Retroviruses* 2002; **18**: 1239-1251.
140. Bajaria SH, Kirschner DE. CTL action during HIV-1. In: Tan W-Y, Wu H, editors. Deterministic and Stochastic Models for AIDS Epidemics and HIV Infection with Intervention: World Scientific Publisher, 2005:219-254.

141. Haase AT. Population biology of HIV-1 infection: viral and CD4+ T cell demographics and dynamics in lymphatic tissues. *Annu Rev Immunol* 1999;**17**:625-56.
142. Rosenberg Y, Anderson A, Pabst R. HIV-induced decline in blood CD4/CD8 ratios: viral killing or altered lymphocyte trafficking? *Immunol Today* 1998; **19**: 10-16.
143. Barron M, Blyveis N, Palmer B, MaWhinney S, Wilson C. Influence of plasma viremia on defects in number and immunophenotype of blood dendritic cell subsets in human immunodeficiency virus 1-infected individuals. *J Infect Dis* 2003; **187**: 26-37.
144. Wigginton JE, Kirschner D. A model to predict cell-mediated immune regulatory mechanisms during human infection with *Mycobacterium tuberculosis*. *J Immunol* 2001;**166**(3):1951-67.
145. Holt PG, Schon-Hegrad MA. Localization of T cells, macrophages and dendritic cells in rat respiratory tract tissue: implications for immune function studies. *Immunology* 1987; **62**(3): 349-56.
146. Stone KC, Mercer RR, Gehr P, Stockstill B, Crapo JD. Allometric relationships of cell numbers and size in the mammalian lung. *Am J Respir Cell Mol Biol* 1992;**6**(2):235-43.
147. Antony VB, Godbey SW, Kunkel SL, Hott JW, Hartman DL, Burdick MD, *et al*. Recruitment of inflammatory cells to the pleural space. Chemotactic cytokines, IL-8, and monocyte chemotactic peptide-1 in human pleural fluids. *J Immunol* 1993;**151**(12):7216-23.
148. Mercer RR, Russell ML, Roggli VL, Crapo JD. Cell number and distribution in human and rat airways. *Am J Respir Cell Mol Biol* 1994;**10**(6):613-24.
149. Law K, Weiden M, Harkin T, Tchou-Wong K, Chi C, Rom WN. Increased release of interleukin-1 beta, interleukin-6, and tumor necrosis factor-alpha by bronchoalveolar cells lavaged from involved sites in pulmonary tuberculosis. *Am J Respir Crit Care Med* 1996;**153**(2):799-804.
150. Condos R, Rom WN, Liu YM, Schluger NW. Local immune responses correlate with presentation and outcome in tuberculosis. *Am J Respir Crit Care Med* 1998;**157**(3 Pt 1):729-35.
151. Young AJ, Hay J. Lymphocyte migration in development and disease. *Semin Immunol* 1999;**11**(2):71.
152. Young AJ. The physiology of lymphocyte migration through the single lymph node in vivo. *Semin Immunol* 1999;**11**(2):73-83.
153. Holt PG. Antigen presentation in the lung. *Am J Respir Crit Care Med* 2000; **162**(4 Pt 2): 151-156.
154. Kepler TB, Perelson AS. Drug concentration heterogeneity facilitates the evolution of drug resistance. *Proc Natl Acad Sci U S A* 1998;**95**(20):11514-9.
155. Kirschner D, Webb GF, Cloyd M. Model of HIV-1 disease progression based on virus-induced lymph node homing and homing-induced apoptosis of CD4+ lymphocytes. *J Acquir Immune Defic Syndr* 2000;**24**(4):352-62.
156. Snedecor SJ. Comparison of three kinetic models of HIV-1 infection: implications for optimization of treatment. *J Theor Biol* 2003;**221**(4):519-41.

157. Ogg G, Jin X, Bonhoeffer S, Rod Dunbar P, Nowak M, Monard S, *et al.* Quantitation of HIV-1-specific cytotoxic T lymphocytes and plasma load of viral RNA. *Science* 1998; **279**: 2103-2106.
158. Scott-Algara D, Buseyne F, Blanche S, Rouzioux C, Jouanne C, Romagne F, *et al.* Frequency and phenotyping of human immunodeficiency virus (HIV)-specific CD8+ T cells in HIV-infected children, using major histocompatibility complex class I peptide tetramers. *J Infect Dis* 2001; **183**: 1565-1573.
159. Vlachos DG. A review of multiscale analysis: Examples from systems biology, materials engineering, and other fluid-surface interacting systems. *Adv. Chem. Eng.* 2005:30-31.
160. Kirschner D. The multi-scale immune response to pathogens: M. tuberculosis as an example. In: Flower D, Timmis J, editors. *In silico Immunology*. New York: Springer, 2006 (in press).
161. Coveney PV, Fowler PW. Modelling biological complexity: a physical scientist's perspective. *J. R. Soc. Interface* 2005(2):267-280.
162. Garny A, Noble D, Kohl P. Dimensionality in cardiac modelling. *Prog Biophys Mol Biol* 2005;**87**(1):47-66.
163. Pai RK, Convery M, Hamilton TA, Boom WH, Harding CV. Inhibition of IFN-gamma-induced class II transactivator expression by a 19-kDa lipoprotein from *Mycobacterium tuberculosis*: a potential mechanism for immune evasion. *J Immunol* 2003;**171**(1):175-84.
164. Gehring AJ, Rojas RE, Canaday DH, Lakey DL, Harding CV, Boom WH. The *Mycobacterium tuberculosis* 19-kilodalton lipoprotein inhibits gamma interferon-regulated HLA-DR and Fc gamma R1 on human macrophages through Toll-like receptor 2. *Infect Immun* 2003;**71**(8):4487-97.
165. Fulton SA, Reba SM, Pai RK, Pennini M, Torres M, Harding CV, *et al.* Inhibition of major histocompatibility complex II expression and antigen processing in murine alveolar macrophages by *Mycobacterium bovis* BCG and the 19-kilodalton mycobacterial lipoprotein. *Infect Immun* 2004;**72**(4):2101-10.
166. Pai RK, Pennini ME, Tobian AA, Canaday DH, Boom WH, Harding CV. Prolonged toll-like receptor signaling by *Mycobacterium tuberculosis* and its 19-kilodalton lipoprotein inhibits gamma interferon-induced regulation of selected genes in macrophages. *Infect Immun* 2004;**72**(11):6603-14.
167. FDA. Critical Path Initiative - <http://www.fda.gov/oc/initiatives/criticalpath>.
168. Donnes P, Elofsson A. Prediction of MHC class I binding peptides, using SVMHC. *BMC Bioinformatics* 2002;**3**:25.
169. Hattotuagama CK, Guan P, Doytchinova IA, Zygouri C, Flower DR. Quantitative online prediction of peptide binding to the major histocompatibility complex. *J Mol Graph Model* 2004;**22**(3):195-207.
170. Hobohm U, Scharf M, Schneider R, Sander C. Selection of representative protein data sets. *Protein Sci* 1992;**1**(3):409-17.
171. Mika S, Rost B. UniqueProt: Creating representative protein sequence sets. *Nucleic Acids Res* 2003;**31**(13):3789-91.
172. Peng G. Mathematical Modeling, Simulation and Analysis Program Area - <http://www.nibib.nih.gov/publicPage.cfm?pageid=1228>. National Institute of Biomedical Imaging and Bioengineering website.

173. Finney A, Hucka M. Systems biology markup language: Level 2 and beyond. *Biochem Soc Trans* 2003;**31**(Pt 6):1472-3.
174. Lloyd CM, Halstead MD, Nielsen PF. CellML: its future, present and past. *Prog Biophys Mol Biol* 2004;**85**(2-3):433-50.
175. Webb K, White T. UML as a cell and biochemistry modeling language. *Biosystems* 2005;**80**(3):283-302.
176. Pai RK, Askew D, Boom WH, Harding CV. Regulation of class II MHC expression in APCs: roles of types I, III, and IV class II transactivator. *J Immunol* 2002;**169**(3):1326-33.